FACULTY OF SCIENCE

SCHOOL OF CHEMISTRY

Photocatalytic degradation of methyl violet using modified radially aligned nano rutile TiO_2-nanodiamonds composite

By

MUGADZA FARIRAI (1951606)

Supervisor: Dr John Moma

Co-supervisors: Prof Nosipho Moloto and Dr Ella Linganiso

Dissertation submitted in fulfilment of the requirements for the degree of Master of Science in Chemistry

2020

Declaration

I declare that this dissertation is my own unaided work. Where the use of the works of other researchers has been made, it has been acknowledged in the text. It is being submitted for the Masters of Science degree in the University of the Witwatersrand, Johannesburg. It has not been submitted before for any degree or examination in any other University.

Signature of Candidate

on the 19th day of April 2020

Dedication

This work is dedicated to my newborn daughter Mukundi, my husband and my family

Acknowledgements

- I would like to thank my supervisors Dr John Moma, Prof. Nosipho Moloto and Dr Cebisa Linganiso for the guidance, patience and support throughout my research.
- I would also like to thank NRF, Thuthuka grant for funding this research in 2019.
- I also extend lots of thanks to Dr Farai Dziike for his assistance in photocatalytic degradation studies and guidance in writing this dissertation, Dr Rudolph Erasmus for his assistance in Raman spectroscopy analyses at the Microscopy and Microanalysis Unit (MMU). Many thanks to the rest of the MMU staff for their assistance and guidance in microscopy sample analysis.
- My special thanks go to the School of Chemistry and CATMAT group for their support, technical assistance and guidance during the period of my research. I would also like to thank my fellow researchers in lab 117 and 330 for their assistance and constructive criticism towards my work.
- Finally, I would like to thank my family and friends for their love and emotional support during the period of my studies.

Abstract

In this work, a hydrothermal method was used to synthesize the radially aligned nano rutile (RANR) TiO_2, using $TiCl_4$ as a precursor. The synthesis temperatures, as well as the time involved in the refluxing step of the synthesis were varied to obtain the optimum morphology of the resulting TiO_2. The optimum refluxing time for RANR TiO_2 synthesis was determined to be 16 hours at 180 °C. The synthesized RANR TiO_2 with dandelion-like shapes had diameters ranging from 300 nm to 800 nm and an average diameter of 560 nm. The RANR TiO_2 had BET surface area of 68 m^2/g, which is higher than that of the commercially available Degussa P25 (45 m^2/g). The RANR TiO_2-nanodiamond composites were all synthesized in situ using the hydrothermal method with detonation nanodiamonds ranging from 0.1 to 1% mass loading. BET surface area analysis showed an increase in the surface area of the RANR TiO_2 with an increase in the amount of nanodiamonds used in its modification. Raman spectra confirmed the presence of graphitic carbon and rutile TiO_2 in all the composite samples. The results obtained from XPS analysis showed that oxygen, carbon and titanium were all present in the sample but there was no evidence showing bond formation between titanium and carbon.

RANR TiO_2 was the most effective in dye degradation due to their nano rod structure, which increases light harvesting properties due to multiple reflections of light. All the other composites did generally well with respect to dandelions in the first hour, but then the rate of degradation decreased which could be attributed to the reduction in photocatalytic active sites due to blockage by reactants. A good dispersion of the nanodiamonds and RANR TiO_2 (0.1% loading) helped to create strong electronic interphase interactions. This helps to separate the photogenerated electrons and positive holes, thereby increasing photocatalytic efficiency. Calcination increased photocatalytic efficiency because of the increase in crystallinity of

materials which reduces electron/hole recombination, the increase in crystallinity was shown by results from Raman spectroscopy. The photocatalyst recyclability studies showed that the recovery of the catalyst after each cycle and the re-use was not effective as the degradation efficiency decreased from 80% to 60% after 3 cycles.

List of figures

List of tables

List of Abbreviations

BE	Binding Energy
BET	Brunauer-Emmett-Teller
CB	Conduction Band
Eg	Band gap energy
FTIR	Fourier transform infrared spectroscopy
GC	Gas Chromatography
KE	Kinetic Energy
PL	Photoluminescence spectroscopy
RANR	Radially Aligned Nano-Rutile
SEM	Scanning Electron Microscope
TEM	Transmission Electron Microscope
TGA	Thermogravimetric Analysis
UNICEF	United Nations Children's Emergency Fund
VB	Valence Band
WHO	World Health Organization
XPS	X-ray Photoelectron Spectroscopy
XRD	X-Ray Diffraction

Contents

Chapter1: Introduction

1.1 Background information

The increase in the growth of industries over the past few years has had a negative effect on the environment in terms of pollution. Water pollution is one of the major concerns as some people do not have access to clean water supplies, especially in developing countries. The discharge of untreated waste water into water bodies is also a concern, since it affects both ground and surface water[1]. A joint monitoring program by the World Health Organization (WHO) and the United Nations Children's Emergency Fund (UNICEF) released a report on the progress of drinking water, sanitation and hygiene in 2017[2]. This report stated that, in 2015, 29% of the global population did not have easy access to safe drinking water that is free from contamination. One out of four people still used contaminated water sources[2]. WHO also predicts that by 2025, almost half of the world's population will be occupying water stressed areas, hence there is a need to come up with cost effective methods of water purification so that contaminated water can be re-used for several cycles[2].

Conventional water treatment methods that are being used are chemical precipitation, ion-exchange adsorption, electro-deposition and membrane systems, among others[3]. The main challenge with these methods is that they use quite expensive technologies, especially for large volumes of water. Photocatalysis is a cost-effective method for purification of water contaminated with organic dyes. Textile, paper and leather tanning industries are the highest contributors of dye waste[3,4]. Since the discovery of nano materials, researchers have been trying to control the architecture of TiO_2 down to nano scale dimensions in order to form different morphologies. Nano dimensional TiO_2 has the advantage of possessing unique properties and

superior performance with potential in various applications including catalysis[5]. Several morphologies have been synthesized which include nano flowers, rods, tubes and wires [6]. TiO_2 is cheap, readily available, environmentally friendly, mechanically and thermally stable, as a result, it can be used for different applications[7].

Photocatalysis is the use of light to activate a catalyst, which then facilitates a chemical reaction. Irradiation of a semiconductor, e.g. TiO_2, with light that has energy higher than its band results in photon absorption and excitation of an electron from the valence band (VB) to the conduction band (CB). This leads to the formation of photogenerated holes in the VB. The excited electron and the generated positive hole can undergo recombination and the excess energy is lost through non-radiative mechanisms[8]. Several methods of modifying TiO_2 have been applied in order to improve its photocatalytic activity. These methods work by reducing the rapid recombination of photo generated electron/hole pairs, poor activation of TiO_2 by visible light and backward reactions[9]. Researchers have tried to enhance the catalytic performance of TiO_2 by metal loading[19,20], dye sensitization[21], metal ion doping[22,23], the use of semiconductor composites[24,25,26] and carbonate salts[10,27,28]. Electron donors, hole scavengers or sacrificial agents such as organic compounds can be used to react irreversibly with the holes in order to reduce electron-hole recombination, thereby increasing quantum efficiency[11].

Nanodiamonds are a relatively new class of materials obtained as a waste material from the detonation of carbon-containing explosives[12]. They are gaining interest in many applications, due to their properties, which include the size ranging from 2 -10 nm. Also, they are a mixture of sp^2 and sp^3 carbon, which can result in different behaviors as compared to other sources of carbon[13]. It has been recently discovered that these nanodiamonds exhibit photocatalytic

activity[14]. The use of carbon to modify TiO_2 could increase its photo response in the visible spectrum[15].

1.2 Problem statement

TiO_2 is a semiconductor with the band structure suitable for photocatalysis; but, it has less photocatalytic driving force due to the relatively positive CB of TiO_2. The other problems associated with TiO_2 are the recombination of photo generated electron/hole pairs, poor activation by visible light and backward reactions. TiO_2 utilizes mostly UV light for photocatalysis, instead of visible light. This limits its application in photocatalysis, because UV light constitutes only 4% of the solar radiation compared to visible light constitutes which 50% of the solar radiation level[9].

1.3 Justification

The TiO_2 photocatalyst is cost effective, readily available, environmentally friendly, non-toxic, mechanically and thermally stable[11]. Radially aligned nano rutile TiO_2 has high surface area compared to other nano morphologies and the commercially available P25[16]. Nano diamonds are a promising material in photocatalysis, and they are obtained as a waste material in carbon-containing explosives, hence there is a need to find novel applications for the material. Also, nano-diamonds have the potential to be applied in composite synthesis, due to their unique chemical, structural and mechanical properties[17]. The use of carbon to modify TiO_2 could increase its photo response into the visible spectrum, thereby increasing the activation of the catalyst. Photocatalysis is a cost effective method for purification of water contaminated with organic dyes, compared to other methods[18].

1.4 Aims and objectives

The aim of this research is to investigate the effect of modifying RANR TiO_2 with nanodiamonds on its physical and chemical properties, as well as in its photocatalytic property. The specific objectives are:

i. Synthesis of RANR TiO_2 using the hydrothermal method
ii. Optimize RANR TiO_2 synthesis condition by varying refluxing time and temperature
iii. In-situ modification of RANR TiO_2 with different amounts of nano diamonds
iv. Characterization of the catalysts for structural, morphological and optical properties using XRD, TEM, SEM, Solid state UV-Vis, PL and Raman spectroscopy.
v. Photocatalytic dye degradation using the synthesized composites

1.5 Research questions

The questions below should be addressed to fulfill the aim of this research:

i. How does temperature affect the synthesis of radially aligned nano rutile?
ii. Does the formation and growth of the nano rods lead to an increase in surface area of the photo catalyst?
iii. Can nanodiamond modification of TiO_2 increase its photo response into the visible spectrum?
iv. Can the TiO_2-nanodiamond improve the photocatalytic performance of TiO_2?

1.6 Dissertation Outline

- Chapter 1: Introduction

  Chapter 1 is an introduction which describes the background information, aims, objectives and research hypothesis of this study. The problems in water purification

methods and the shortcomings of TiO_2 as a photocatalyst were discussed as well as the justification for the choice of materials under study.

- Chapter 2: Literature review

  This chapter gives a detailed literature review on the progress made in modifications of TiO_2 for enhanced photocatalysis. The chapter discusses the work that has been done by other researchers on the synthesis methods of TiO_2, modification of TiO_2 by various methods and application of the materials in photocatalysis.

- Chapter 3: Methodology

  This chapter explains the hydrothermal synthesis of the catalysts, step by step, including the reaction setups for the synthesis and application of the synthesized photocatalysts. It also gives a detailed description on the theories of the instruments that were used for characterization and dye degradation.

- Chapter 4: Characterization results

  Chapter 4 describes the results obtained from several characterization techniques that were used in this study.

- Chapter 5: Application in photocatalysis

  Chapter 5 describes the trends observed in the photocatalytic degradation of methyl violet by the synthesized catalysts. Rate of degradation of the organic dye was used to compare the efficiencies of the photocatalysts.

- Chapter 6: Results summary

This chapter summarized the characterization results obtained and the photocatalytic activity of RANR TiO_2- nanodiamonds composites.

- Chapter 7: Conclusion and future studies

Concluding statements as well as future direction and perspectives were suggested.

1.7 References

1. Pelaez M, Nolan NT, Pillai SC, A review on the visible light active titanium dioxide photocatalysts for environmental applications. *Appl Catal B Environ*. 2012; 125: 331-349.
2. WHO, UNICEF. *Progress on Drinking Water, Sanitation and Hygiene 2017*.; 2017. https://washdata.org/sites/default/files/documents/reports/2018-01/JMP-2017-report-final-highlights.pdf.
3. Gaya UI, Abdullah AH. Heterogeneous photocatalytic degradation of organic contaminants over titanium dioxide: A review of fundamentals, progress and problems. *J Photochem Photobiol C Photochem Rev*. 2008; 9(1): 1-12.
4. Konstantinou IK, Albanis TA. TiO_2-assisted photocatalytic degradation of azo dyes in aqueous solution: Kinetic and mechanistic investigations: A review. *Appl Catal B Environ*. 2004; 49(1): 1-14.
5. Bai X, Xie B, Pan N, Wang X, Wang H. Novel three-dimensional dandelion-like TiO_2 structure with high photocatalytic activity. *J Solid State Chem*. 2008; 181(3): 450-456.
6. Bai Y, Liu Z, Zhang N, Sun K. One-pot synthesis of 3-D dandelion-like architectures constructed by rutile TiO_2 nanorods grown along [001] axis for high-rate lithium ion batteries. *RSC Adv*. 2015; 5(27): 21285-21289.
7. Baloyi J, Seadira T, Raphulu M, Ochieng A. Synthesis and Characterization of Dandelion-like TiO_2 Structure as Photocatalyst for Industrial Wastewater Treatment Containing Toxic Metal Hg (II). *PsrcentreOrg*. 2014; (Ii). http://psrcentre.org/images/extraimages/414028.pdf.
8. Banerjee S, Pillai SC, Falaras P, O'shea KE, Byrne JA, Dionysiou DD. New insights into the mechanism of visible light photocatalysis. *J Phys Chem Lett*. 2014; 5(15): 2543-2554.
9. Gupta SM, Tripathi M. A review of TiO_2 nanoparticles. *Chinese Sci Bull*. 2011; 56(16):

1639-1657.

10. Hashimoto K, Irie H, Fujishima A. TiO_2 Photocatalysis: A Historical Overview and Future Prospects. *Jpn J Appl Phys*. 2005; 44(12): 8269-8285.
11. Ni M, Leung MKH, Leung DYC, Sumathy K. A review and recent developments in photocatalytic water-splitting using TiO_2 for hydrogen production. *Renew Sustain Energy Rev*. 2007; 11(3): 401-425.
12. Dolmatov V. Detonation Nanodiamonds. *Carbon Nanomater Sourceb*. 2016: 509-524. doi:10.1201/b19679-26
13. Sitnikova AA, Vul AY, Efimov ON, Bakaev VA, Aleksenskii AE. Detonation Nanodiamonds as Catalyst Supports. 2010; 4046. doi:10.1080/1536383X.2010.490143
14. Jang DM, Myung Y, Im HS. Nanodiamonds as photocatalysts for reduction of water and graphene oxide. *Chem Commun*. 2012; 48(5): 696-698.
15. Park JH, Kim S, Bard AJ. Novel Carbon-Doped TiO_2 Nanotube Arrays with High Aspect Ratios for Efficient Solar Water Splitting. *Nano Lett*. 2006; 6(1): 24-28.
16. Baloyi J, Seadira T, Raphulu M, Ochieng A. Preparation, Characterization and Growth Mechanism of Dandelion-like TiO_2 Nanostructures and their Application in Photocatalysis towards Reduction of Cr(VI). *Mater Today Proc*. 2015; 2(7): 3973-3987.
17. Lin Z, Xiao J, Li L, Liu P, Wang C, Yang G. Nanodiamond-Embedded p-Type Copper(I) Oxide Nanocrystals for Broad-Spectrum Photocatalytic Hydrogen Evolution. *Adv Energy Mater*. 2016; 6(4): 1-10.
18. Ahmad H, Kamarudin SK, Minggu LJ, Kassim M. Hydrogen from photo-catalytic water splitting process: A review. *Renew Sustain Energy Rev*. 2015; 43: 599-610.
19. Devi LG, Kavitha R. A review on non metal ion doped titania for the photocatalytic degradation of organic pollutants under UV/solar light: Role of photogenerated charge carrier dynamics in enhancing the activity. *Appl Catal B Environ*. 2013; 140-141: 559-587.
20. Barrett DH, Scurrell MS, Rodella CB, Diaz B, Billing DG, Franklyn PJ. Achieving nano-gold stability through rational design. *Chem Sci*. 2016; 7(11): 6815-6823.
21. Beretta A, Bruno T, Groppi G, Tavazzi I, Forzatti P. Conditioning of Rh-Al_2O_3 catalysts for H_2 production via CH_4 partial oxidation at high space velocity. 2007; 70: 515-524. doi:10.1016/j.apcatb.2006.01.014
22. Ismail AA, Bahnemann DW. Photochemical splitting of water for hydrogen production

by photocatalysis: A review. *Sol Energy Mater Sol Cells*. 2014; 128: 85-101.

23. Xu AW, Gao Y, Liu HQ. The preparation, characterization, and their photocatalytic activities of rare-earth-doped TiO_2 nanoparticles. *J Catal*. 2002; 207(2): 151-157.

24. Ni M, Leung MKH, Leung DYC, Sumathy K. A review and recent developments in photocatalytic water-splitting using TiO_2 for hydrogen production. *Renew Sustain Energy Rev*. 2007; 11(3): 401-425.

25. Sampaio MJ, Pastrana-Martinez LM, Silva AMT. Nanodiamond TiO_2 composites for photocatalytic degradation of microcystin-LA in aqueous solutions under simulated solar light. *RSC Adv*. 2015; 5(72): 58363-58370.

26. Yu J, Ran J. Facile preparation and enhanced photocatalytic H2-production activity of $Cu(OH)_2$ cluster modified TiO_2. *Energy Environ Sci*. 2011; 4(4): 1364.

27. Ahmad H, Kamarudin SK, Minggu LJ, Kassim M. Hydrogen from photo-catalytic water splitting process: A review. *Renew Sustain Energy Rev*. 2015; 43: 599-610.

28. Ohno T, Tsubota T, Nishijima K, Miyamoto Z. Degradation of Methylene Blue on Carbonate Species-doped TiO_2 Photocatalysts under Visible Light. *Chem Lett*. 2004; 33(6): 750-751.

Chapter 2: Literature review

TiO_2 is a semiconductor, which is also a transition metal oxide. It exists naturally in three polymorphs, which are rutile, anatase and brookite. Both anatase and rutile have a tetragonal structure, whereas brookite is orthorhombic[1]. The polymorphs have different bandgaps which are 2.96, 3.02 and 3.20 eV for brookite, rutile and anatase respectively. Rutile is the most stable polymorph at most temperatures and pressure. The activity of the rutile phase as a photo catalyst depends mainly on the synthesis method[2]. The photocatalytic activity of TiO_2 was first discovered in the early 20th century, where it was found to be highly active under UV light irradiation[3]. TiO_2 is cheap, readily available, environmentally friendly, non-toxic, mechanically and thermally stable, therefore it can be used for different applications[4], which include pharmaceuticals, cosmetics, food colorants, automotive products, paints, adhesives and catalysis[5].TiO_2 was found to be one of the best materials suitable for photocatalysis because its photogenerated holes are strongly oxidising and redox selective[6]. Some major drawbacks of TiO_2 have been discovered over the decades such as its poor visible photo response and the rapid recombination of photo generated electron/hole pairs[2].

2.1 TiO_2 modification

The drawbacks of TiO_2 as a photocatalyst can be overcome by anion doping, dye sensitization, noble metal loading, semiconductor composite, co-doping, capping, doping with metalloids, hybridization and metal ion implantation[7]. Preliminary studies have shown that sacrificial agents/ hole scavengers/ electron donors and carbonate salts can be used to react irreversibly with the photogenerated holes thereby reducing electron/ hole recombination which in turn increases quantum efficiency[6].

2.1.1 Radially aligned nano rutile (RANR) TiO_2

Nano dimensional TiO_2 has the advantage of possessing unique properties and superior performance with potential in various applications, including catalysis[8]. A lot of research has been undertaken to control the architecture of titanium dioxide, down to nano scale dimensions with different morphologies. Several morphologies have been synthesized such as nano flowers, rods, tubes and wires. RANR TiO_2 or dandelion-like titania is three dimensional and has a high surface area. This can impact positively on a variety of economically important technologies, especially in catalysis[9].

Rutile 3D dandelion-like nanostructures were synthesized by a facile hydrothermal method using $TiCl_3$ as the source of titania. The effects of synthesis parameters, i.e. reaction time, synthesis temperature and pH on the morphology and crystal phase of TiO_2 were investigated. Dandelions with an average diameter of 1.5 to 2 μm were synthesized at temperatures between 180 °C and 190 °C[8]. An increase in reaction time from 180 to 240 minutes and synthesis temperatures between 180 °C and 190 °C, both increased the packing of nanorods to give denser and compact dandelions. At pH less than 3 the formation of dandelions was favoured, while an increase of pH from 3-5 reduced packing of the nanorods. A further increase of the pH above 7 led to the formation of irregular nanorods[8]. Xuelian et al. showed that the nano rods growth occurred via three steps, which are precipitation of TiO_2 nanoparticles in solution due to homogeneous nucleation, followed by the aggregation of the nano rods and finally densely packed mature dandelions. They also suggested that in the nucleation and growth mechanism, some newly nucleated nano rods which grow along the radial direction, misaligned with respect to the originally aggregated nano rods, promote the growth of dense mature nano rods[8].

Dandelion-like rutile TiO_2 was also synthesized using the solvothermal method, with titanium-n-butoxide (TNB) as the starting material or source of titania. The effect of increasing synthesis temperature and TNB concentration on the morphology was studied. TNB concentrations of less than 0.2 M led to a collapse of the dandelion structure, whereas concentrations between 0.3 M and 0.5 M gave the best dandelion-like structures. Increasing the reaction temperatures from 120 °C to between 150 °C and 180 °C also increased the diameter of the spheres from 1 μm to 1.5 μm, and the diameter of the nanorods from 5 nm to 10 nm. A further increase in reaction temperature to 210 °C also increased the diameter of the spheres to 1-2.5 μm, as well as the diameters of the nanorods to 35 nm[10]. Dandelion-like structures with tapered tips showed higher photocatalytic efficiency as compared to the ones with flat tops. The interspaces between the nano rods act as light transfer channels and the tapered tip geometry favors lower reflectance which leads to high absorption of light hence efficient light harvesting which is a good property especially in photocatalysis [10].

The hydrothermal method was used to synthesize dandelion-like TiO_2 using hollow SnO_2 spheres using toluene as a non-polar solvent for titanium (IV) butoxide. HCl was used to avoid precursor hydrolysis. Jin Yi et al. suggested that TiO_2 crystal nuclei formed on the surface of the SnO_2 spheres, the nanorods then grew towards the center of the spheres, thereby dissolving them, leading to the formation of a dandelion-like structure. The synthesized photocatalyst was used for application as anode materials for lithium ion batteries with high rate capacity and cyclic stability. Their good performance was attributed to the morphology, which has high surface areas, as well as the single crystalline building blocks that enhance electrons and lithium ion transport[9].

Baloyi et al. also synthesized dandelion-like TiO_2 using the hydrothermal method with a synthesis temperature of 100 °C and refluxing for 24 hours. Temperatures below 100 °C such as 80 °C yielded loosely packed nanorods, whereas high temperatures of 190 °C destroyed the dandelion structure into TiO_2 sheet-like structures. Scale-up and reproducibility studies were done and the results indicated that increasing the quantities of the starting materials had no significant change on the structural and chemical characteristics of the dandelion-like TiO_2. The synthesized materials showed high photocatalytic activity in the reduction of Cr (VI) as compared to P25. This was attributed to the high light-harvesting properties resulting from multiple reflection of light due to the dandelion-like morphology of the nanorods, as well as high surface areas[11].

2.1.2 Composite semiconductors

Composite semiconductors can be used to increase photocatalytic efficiency of TiO_2. Coupling semiconductors with different band gaps can lead to the injection of CB electrons from semiconductor with a small bandgap to the other with a large band gap. The difference of composite semiconductors from dye sensitization is that injection of electrons occurs between the semiconductors, whereas in dye sensitization, electrons are from an excited dye to the semiconductor. An example of a composite semiconductor is MO_x-ZnO where M represents W, V or Fe. Coupling semiconductors is successful if the semiconductor with the small bandgap can be excited by visible light. Electron injection should be fast and efficient with both the semiconductors being resistant to photo-corrosion and the CB of the semiconductor with the larger bandgap needs to be more negative than $E_{H2/H2O}$ [12].

A nanodiamond-TiO_2 composite was synthesized using a liquid phase deposition procedure for application in photocatalytic degradation of microcystin-LA in aqueous solutions under simulated solar light. Characterization techniques that were used include XRD, TEM, SEM,

DRIFT analysis, DRUV-Vis among others. DRIFT analysis showed the broadening of the TiO_2 band in the composite, which was attributed to the formation of Ti-O-C bond, i.e. a heterojunction was created at the nanodiamond and TiO_2 interface. DRUV-Vis analysis results showed a TiO_2 blue band shift in the composite, which was attributed to the presence of site defects in the TiO_2 crystalline structure, due to the carbon in the nano diamonds. The addition of nanodiamonds was reported to have increased the efficiency of the catalyst in the photocatalytic degradation of microcystin-LA using solar light[13]. This was attributed to the good dispersion of the nano diamonds in the composite, which led to the creation of strong electronic interface interactions[13].

A $CuOH_2$ cluster modified TiO_2 photocatalyst was prepared by precipitation using TiO_2 powder as a support and $Cu(NO_3)_2$ as a precursor[14]. The photocatalytic H_2 production by water splitting was carried out in a pyrex flask at room temperature and atmospheric pressure with the openings of the flask sealed. The gases produced were analyzed by GC. Characterization was done by XRD, UV-Vis, BET and XPS analysis to understand the interactions between the photo generated electrons and holes[14]. The use of $Cu(OH)_2$ clusters increased hydrogen production by reducing electron-hole recombination. This was achieved because copper had a lower conduction band than TiO_2, so electrons could be transferred from the valence band of titania to the conduction band of copper and the electrons were effectively used to reduce protons to give hydrogen gas[14].

2.1.3 Anion doping

Anion doping of titania with anions such as N, F, C and S is an attempt to increase the photo response of titania in the visible spectrum. The anions are more effective as compared to cations, because of the reduced likelihood to form recombination centers. Nitrogen doped TiO_2

was prepared by oxidation of titanium nitride with H_2O_2, hydrothermally. The catalyst was dispersed in the solution by ultra-sonication. An XPA-II photochemical reactor with visible light was used in the study. The nitrogen doped photocatalyst that was prepared with H_2O_2 had excellent stability and was recyclable. Photocatalytic activity increased with increase in H_2O_2 concentration because H_2O_2 oxidized TiN, thereby reducing N content.[17]. Wu X. et al. also used synthesized carbon doped TiO_2 photocatalyst using a facile calcination assisted solvothermal method. The photocatalyst had a high destruction ability of NO gas and also a high degradation ability of methyl orange compared to the commercially available P25. Carbon was doped into the TiO_2 lattice by replacing the oxygen sites with the production of oxygen vacancy. Titanium tetra-n-butoxide was added dropwise to an ethanol/water mixture with continuous stirring. The solution was then transferred to a Teflon-lined stainless-steel autoclave and heated. This was then centrifuged, washed with distilled water and ethanol and then dried at 60 °C overnight. Calcination was then done at different temperatures and the photocatalysts were used for photocatalytic methyl orange degradation and decomposition of NO in a flow type reactor[18].

Three different sources of nitrogen were used to dope TiO_2 which include urea, diethanolamine and triethylamine. Diethanolamine showed the highest visible light absorption ability with the smallest bandgap and the smallest anatase crystal size. A modified sol-gel method was used to synthesize the catalyst using the three different nitrogen sources. For the photocatalysis, a cylindrical reactor made from quartz glass was used where sodium nitride was used as a UV filter to eliminate light with a wavelength less than 420 nm. TiO_2 doped with diethanolamine showed the highest efficiency in 2-chlorophenol photodegradation, due to its high surface area compared to the other doped catalysts. The undoped TiO_2 was the least photocatalytic active

catalyst, this was attributed to the high bandgap energy which led to the formation of less OH radicals as compared to the other catalysts[19].

2.2 Nano diamonds

Nanodiamonds are a zero-dimensional nanocrystalline carbon material with an sp^3 bonded carbon/diamond core. They can be synthesized using various methods, which include laser ablation, detonation of carbon containing explosives, high energy ball milling of diamond microcrystals, chlorination of carbides, electron irradiation of carbon nano onions and plasma assisted CVD[26]. Detonation nanodiamonds have a narrow/ uniform size distribution of 2-7 nm and large surface areas of approximately 300 m^2g^{-1}. Nanodiamonds have a chemically inert diamond (sp^3) core and graphitic (sp^2) carbon shell. The graphitic shell has functional groups attached to it, which include ketones, carboxyl, alkyl and hydroxyl groups[27].

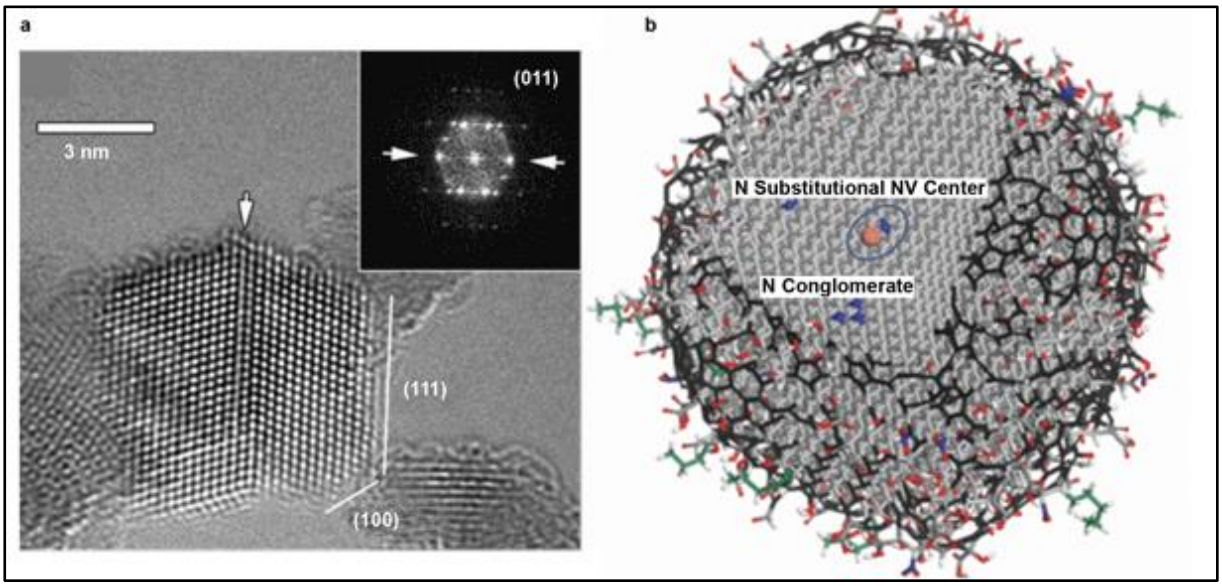

Figure 2.1: HR-TEM image showing the crystallographic structure of the nanodiamond core (a) and (b) shows a model of detonation nanodiamonds with a diamond core in grey and sp^2 hybridized carbon in black with different functional groups[28].

Detonation nanodiamonds contain several impurities like metals and other sp^2 carbon materials. Acidic treatment can be used to remove the metallic impurities, whereas HNO_3/H_2O_2

can be used under pressure to remove other forms of carbon[29]. Nanodiamond surface groups present depend on the purification method used. Raman spectroscopy has been used in literature to provide important information but intense signals can arise due to the presence of impurities attached to the sp^2 hybridized carbon. Nitrogen is the most common impurity which occurs in the form of substituted carbon atoms[30]. The nitrogen atoms can have vacant sites adjacent to them which are termed N-vacant sites. These N-vacant sites contribute to the luminescent properties of nano diamonds and they have broad emission profiles which makes them suitable for applications such as biomedical imaging[31].

Nanodiamonds possess some of the properties of bulk diamonds which are hardness, optical properties, biocompatibility, chemical stability, high thermal conductivity and resistance to harsh environments. They also have unique mechanical and electronic properties. The unique properties of nano diamonds make them useful in various applications, which are nanocomposites, drug delivery, magnetic sensing, catalysis and electrochemistry[32]. Detonation nanodiamonds (obtained from carbon containing explosives) with an average diameter of 5nm were reported to show photocatalytic activity. They were used for H_2 production by reduction of water using laser pulse irradiation and were also used to reduce graphene oxide. Treatment of the nanodiamonds with hydrogen increased their photocatalytic efficiency and this was attributed to the H-terminated sites which acted as electron reservoirs[33].

2.3 Nanodiamond-TiO_2 Composite

The presence of functional groups on the graphitic shell of the nanodiamonds makes surface modification a possibility, which is important in composite synthesis[33]. Combining TiO_2 with other carbon materials has been proven to increase photocatalytic efficiency. This is due to the formation of an interfacial electron transfer layer between TiO_2 and the carbon, which increases

the light harvesting ability of TiO_2 optimizing quantum yield hence increased photocatalytic efficiency[34].

Liquid phase deposition was used in the synthesis of nanodiamonds and TiO_2 composite and the composite was used for application in the degradation of microcystin-LA using photocatalysis[13]. A 15-weight percent of oxidized nano diamonds (confirmed by TGA) was used to modify the TiO_2. A decrease in BET surface area from 118 m^2/g to 81 m^2/g was reported, as well as an increase in crystallite size of the TiO_2 from 8 nm in pure TiO_2 to 11 nm in the composite. This was attributed to the competition of TiO_2 species on the oxidized nano diamonds surface during synthesis, thereby increasing the size of TiO_2. There was an increased photocatalytic efficiency under solar simulation, which was attributed to a good dispersion of the nano diamonds and TiO_2, which led to an electronic interaction at the heterojunction interface between the two materials[13].

Another composite of TiO_2 and nanodiamonds was prepared by atomic layer deposition. Micro diamonds (1-2 μm) and nanodiamonds (2-10 nm) were combined with TiO_2 and their photocatalytic activity was compared[34]. The composite with a 15 wt% of nanodiamonds oxidized at 703K showed an increase in photocatalytic activity in the degradation of diphenhydramine under UV-Vis irradiation. The oxidation of the nanodiamonds gave rise to the formation of new functional groups on their surface which included carboxylic acids, anhydrides, lactones and phenols[34]. Hydrogen, oxygen treated and acid purified nanodiamonds were prepared and their photocatalytic activity towards hydrogen production by reduction of water was tested using 532 laser pulse irradiation accompanied by a multiphoton absorption process. FTIR data obtained proved that oxygenation of nanodiamonds increased carbon-oxygen double bonds, whereas hydrogenation decreased them. The hydrogenation of nanodiamonds increased hydrogen production, i.e. quantum yield, which suggested that

hydrogen terminated sites acted as electron reservoirs[35;29]. This was referred to as the ‘‘transfer doping’’ model.

2.4 Photocatalysis

Photocatalysis is the acceleration of a reaction by irradiation of light to a catalyst that lowers activation energy. Heterogeneous catalysis occurs when the phase of the catalyst is different from that of the reactant. Heterogeneous catalysis occurs in five steps which are the transfer of reactants to the catalyst surface, adsorption of reactants on the catalyst surface (TiO_2), reaction in the adsorbed phase, i.e. photocatalysis, desorption of the products and finally, removal of the products from the interface region. Absorption of photons in heterogeneous photocatalysis occurs when the semi-conductor catalyst is illuminated with photons that have energy (E) higher than that of the bandgap (E_g), i.e. $hv \geq E_g$, where hv is the energy of the photons. Heterogeneous photocatalysis is important due to its low cost since the catalyst is easy to remove after the reaction, both oxidative and reduction reactions occur simultaneously and the use of solar energy, which is a renewable energy resource[36]. It was discovered that TiO_2 was able to degrade organic compounds in the presence of sunlight between the 1970’s and 1980’s[37]. Since then, researchers have been testing the degradation capability of other compounds such as cyanides using TiO_2[38]. Other applications of photocatalysis include hydrogen production (water splitting), antitumor activity (cancer therapy), self-sterilization of hospital floors and air purification among others as shown in figure 2.2.

Figure 2.2: Picture showing applications of TiO_2 in photocatalysis[2].

Photocatalytic degradation of organic dye pollutants is one of the applications of TiO_2. The equations below show the photocatalytic dye degradation mechanism;

Semiconductor (TiO_2) + light (hv) $\longrightarrow$ electrons + positive hole (1)

$H_2O + h^+ \longrightarrow 2OH^- + 2H^+$ (2)

$OH^- + h^+ \longrightarrow OH\cdot$ (3)

$O_2 + e^- \longrightarrow O_2^-$ (4)

$H_2O + O_2 + 2e^- \longrightarrow H_2O_2$ (5)

$H_2O_2 + e^- \longrightarrow OH\cdot + OH^-$ (6)

Methyl violet $\xrightarrow{O_2^- \text{ or } OH\cdot}$ $CO_2 + H_2O$ + other products (7)

The process involves the absorption of light by the photocatalyst (TiO_2) which causes the electron-hole separations, where the electron is excited to the conduction band (1)[39]. This process is called photoexcitation and it only occurs if the energy of the photons (hv) is greater than or equal to the band gap energy. Photoexcitation leads to the formation of positive holes

(h^+) in the valence band. The positive hole reacts with water to give OH^- and OH radicals (2 and 3), i.e. ionization of water[40]. Oxygen ionosorption also occurs, where the excited electrons react with oxygen to give the anion radical superoxide (4), which also oxidizes the organic dye to give carbon dioxide and water (7)[41,1,42]. Hydrogen peroxide can also be produced from the reaction of water and oxygen in the presence of electrons (5). H_2O_2 can be further reduced to form OH radicals which can be used to attack the organic dye to give CO_2 and H_2O, hence water purification (7).

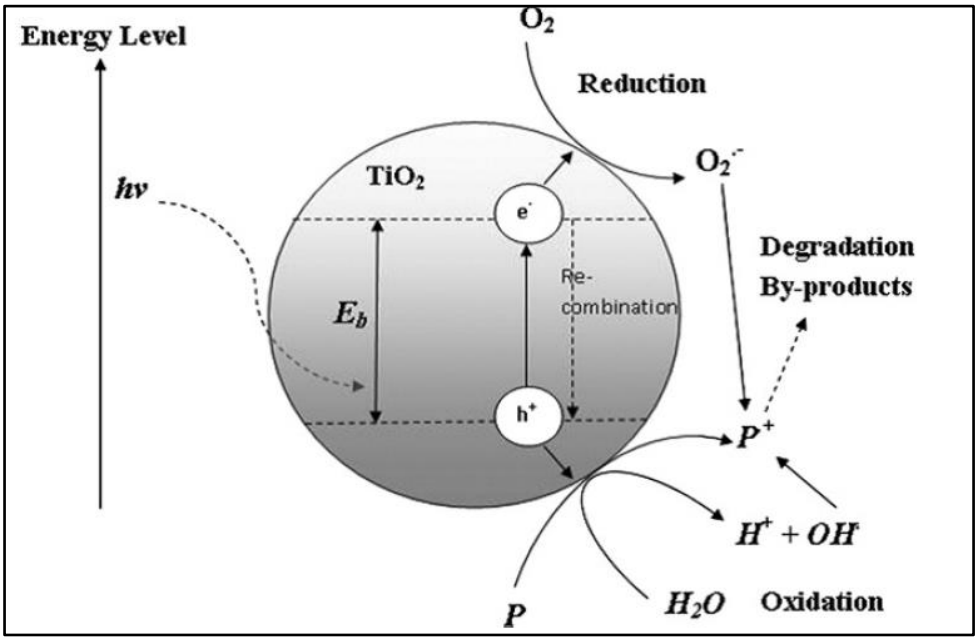

Figure 2.3: The mechanism of photocatalytic organic dye degradation[40].

Factors affecting photocatalytic efficiency are size, surface area, pore volume, crystalline phase, pore structure and the exposed surface facets of the semiconductor photocatalyst[43]. Structural dimensionality of the photocatalyst also affects the efficiency of the photocatalyst, e.g. 0-D, 1-D, 2-D or 3-D structures. 0-D structures, e.g. spheres and one-dimensional structures such as fibers, which look like a non-woven mat, give rise to less recombination of photogenerated electron holes and photogenerated electrons, due to the short charge carrier diffusion distance and light scattering properties. 2-D structures, e.g. nanosheets have smooth

surfaces and are highly adhesive. 3-D structures, i.e. interconnected structures like the radially aligned nano rutile (RANR) TiO_2 synthesized in this study have high carrier mobility. 3D structures have potentially large surface area- to-volume ratio which gives rise to efficient diffusion pathways for organic pollutants into the semiconductor framework which leads to efficient purification[43].

2.5 References

1. Pelaez M, Nolan NT, Pillai SC. A review on the visible light active titanium dioxide photocatalysts for environmental applications. *Appl Catal B Environ*. 2012; 125: 331-349.
2. Gupta SM, Tripathi M. A review of TiO_2 nanoparticles. *Chinese Sci Bull*. 2011; 56(16): 1639-1657.
3. Schneider J, Matsuoka M, Takeuchi M, Zhang J, Yu Horiuchi, Anpo M, Bahnemann DW. Understanding TiO_2 Photocatalysis Mechanisms and Materials. *Chemical Review*. 2014; 114 (19): 9919-9986
4. Baloyi J, Seadira T, Raphulu M, Ochieng A. Synthesis and Characterization of Dandelion-like TiO_2 Structure as Photocatalyst for Industrial Wastewater Treatment Containing Toxic Metal Hg (II). *PsrcentreOrg*. 2014; http://psrcentre.org/images/extraimages/414028.pdf.
5. Mosaddeghi H, Rezaei B, Mosaddeghi H. Applications of Titanium Dioxide Nanoparticles. *Appl Titan Dioxide Nanocoatings*. 2009; (1): 1-4.
6. Hashimoto K, Irie H, Fujishima A. TiO 2 Photocatalysis: A Historical Overview and Future Prospects. *Jpn J Appl Phys*. 2005; 44(12): 8269-8285.
7. Ibhadon AO, Fitzpatrick P. Heterogeneous photocatalysis: Recent advances and applications. *Catalysts*. 2013; 3(1):189-218.
8. Bai X, Xie B, Pan N, Wang X, Wang H. Novel three-dimensional dandelion-like TiO_2 structure with high photocatalytic activity. *J Solid State Chem*. 2008; 181(3): 450-456.
9. Yi J, Liu Y, Wang Y, Li X, Hu S, Li W. Synthesis of dandelion-like TiO_2 microspheres as anode materials for lithium ion batteries with enhanced rate capacity and cyclic performances. 2012; 19(11): 1058-1062.
10. Zhou J, Zhao G, Han G, Song B. Solvothermal growth of three-dimensional TiO_2

nanostructures and their optical and photocatalytic properties. *Ceram Int*. 2013; 39(7): 8347-8354.

11. Baloyi J, Seadira T, Raphulu M, Ochieng A. Preparation, Characterization and Growth Mechanism of Dandelion-like TiO_2 Nanostructures and their Application in Photocatalysis towards Reduction of Cr(VI). *Mater Today Proc*. 2015; 2(7): 3973-3987.
12. Ni M, Leung MKH, Leung DYC, Sumathy K. A review and recent developments in photocatalytic water-splitting using TiO_2 for hydrogen production. *Renew Sustain Energy Rev*. 2007; 11(3): 401-425.
13. Sampaio MJ, Pastrana-Martinez LM, Silva AMT. Nanodiamond TiO_2 composites for photocatalytic degradation of microcystin-LA in aqueous solutions under simulated solar light. *RSC Adv*. 2015; 5(72): 58363-58370.
14. Yu J, Ran J. Facile preparation and enhanced photocatalytic H_2-production activity of $Cu(OH)_2$ cluster modified TiO_2. *Energy Environ Sci*. 2011; 4(4): 1364-1375.
15. Ismail AA, Bahnemann DW. Photochemical splitting of water for hydrogen production by photocatalysis: A review. *Sol Energy Mater Sol Cells*. 2014; 128: 85-101.
16. Cong Y, Li X, Qin Y. Carbon-doped TiO_2 coating on multiwalled carbon nanotubes with higher visible light photocatalytic activity. *Appl Catal B Environ*. 2011; 107(1-2): 128-134.
17. Zhou X, Peng F, Wang H, Yu H, Yang J. Preparation of nitrogen doped TiO_2 photocatalyst by oxidation of titanium nitride with H_2O_2. *Mater Res Bull*. 2011; 46(6): 840-844.
18. Wu X, Yin S, Dong Q. Synthesis of high visible light active carbon doped TiO_2 photocatalyst by a facile calcination assisted solvothermal method. *Appl Catal B Environ*. 2013; 142(3): 450-457.
19. Ananpattarachai J, Kajitvichyanukul P, Seraphin S. Visible light absorption ability and photocatalytic oxidation activity of various interstitial N-doped TiO_2 prepared from different nitrogen dopants. *J Hazard Mater*. 2009; 168(1): 253-261.
20. Ahmad H, Kamarudin SK, Minggu LJ, Kassim M. Hydrogen from photo-catalytic water splitting process: A review. *Renew Sustain Energy Rev*. 2015; 43: 599-610.
21. Ohno T, Tsubota T, Nishijima K, Miyamoto Z. Degradation of Methylene Blue on Carbonate Species-doped TiO $_2$ Photocatalysts under Visible Light. *Chem Lett*. 2004; 33(6): 750-751.
22. Devi LG, Kavitha R. A review on non metal ion doped titania for the photocatalytic degradation of organic pollutants under UV/solar light: Role of photogenerated charge

carrier dynamics in enhancing the activity. *Appl Catal B Environ*. 2013; 140-141: 559-587.

23. Ranjit KT, Viswanathan B. Photocatalytic reduction of dinitrogen to ammonia. *Indian J Chem - Sect A Inorganic, Phys Theor Anal Chem*. 1996; 35(6): 443-453.
24. Barrett DH, Scurrell MS, Rodella CB, Diaz B, Billing DG, Franklyn PJ. Achieving nano-gold stability through rational design. *Chem Sci*. 2016; 7(11): 6815-6823.
25. Xu AW, Gao Y, Liu HQ. The preparation, characterization, and their photocatalytic activities of rare-earth-doped TiO_2 nanoparticles. *J Catal*. 2002; 207(2): 151-157.
26. Brown N, Hod O. Controlling the electronic properties of nanodiamonds via surface chemical functionalization: A DFT study. *J Phys Chem C*. 2014; 118 (10): 5530-5537.
27. Dolmatov V. Detonation Nanodiamonds. *Carbon Nanomater Sourceb*. 2016: 509-524. doi:10.1201/b19679-26
28. Mochalin VN, Shenderova O, Ho D, Gogotsi Y. The properties and applications of nanodiamonds. *Nat Nanotechnol*. 2012; 7(1): 11-23.
29. Pichot V, Comet M, Fousson E. An efficient purification method for detonation nanodiamonds. *Diam Relat Mater*. 2008; 17(1): 13-22.
30. Papagiannouli I, Bourlinos AB, Bakandritsos A, Couris S. Nonlinear optical properties of colloidal carbon nanoparticles: Nanodiamonds and carbon dots. *RSC Adv*. 2014; 4(76): 40152-40160.
31. Georgakilas V, Perman JA, Tucek J, Zboril R. Broad Family of Carbon Nanoallotropes: Classification, Chemistry, and Applications of Fullerenes, Carbon Dots, Nanotubes, Graphene, Nanodiamonds, and Combined Superstructures. *Chem Rev*. 2015; 115(11): 4744-4822.
32. Lin Z, Xiao J, Li L, Liu P, Wang C, Yang G. Nanodiamond-Embedded p-Type Copper(I) Oxide Nanocrystals for Broad-Spectrum Photocatalytic Hydrogen Evolution. *Adv Energy Mater*. 2016; 6(4): 1-10.
33. Bogatyreva GP, Marinich MA, Ishchenko E V., Gvyazdovskaya VL, Bazalii GA, Oleinik NA. Application of modified nanodiamonds as catalysts of heterogeneous and electrochemical catalyses. *Phys Solid State*. 2004; 46(4): 738-741.
34. Pastrana-Martínez LM, Morales-Torres S, Carabineiro SAC. Nanodiamond-TiO_2 composites for heterogeneous photocatalysis. *Chempluschem*. 2013; 78(8): 801-807.
35. Jang DM, Myung Y, Im HS. Nanodiamonds as photocatalysts for reduction of water and graphene oxide. *Chem Commun*. 2012; 48(5): 696-698.
36. Litter MI. Heterogeneous photocatalysis: Transition metal ions in photocatalytic

systems. *Appl Catal B Environ*. 1999; 23(2-3): 89-114.

37. Fujishima A, Zhang X, Tryk DA. Heterogeneous photocatalysis: From water photolysis to applications in environmental cleanup. *Int J Hydrogen Energy*. 2007; 32(14): 2664-2672.
38. Herrmann JM. Heterogeneous photocatalysis: Fundamentals and applications to the removal of various types of aqueous pollutants. *Catal Today*. 1999; 53(1): 115-129.
39. Zangeneh H, Zinatizadeh AAL, Habibi M, Akia M, Hasnain Isa M. Photocatalytic oxidation of organic dyes and pollutants in wastewater using different modified titanium dioxides: A comparative review. *J Ind Eng Chem*. 2015; 26: 1-36.
40. Gaya UI, Abdullah AH. Heterogeneous photocatalytic degradation of organic contaminants over titanium dioxide: A review of fundamentals, progress and problems. *J Photochem Photobiol C Photochem Rev*. 2008; 9(1): 1-12.
41. Teh CM, Mohamed AR. Roles of titanium dioxide and ion-doped titanium dioxide on photocatalytic degradation of organic pollutants (phenolic compounds and dyes) in aqueous solutions: A review. *J Alloys Compd*. 2011; 509(5): 1648-1660.
42. Ajmal A, Majeed I, Malik RN, Idriss H, Nadeem MA. Principles and mechanisms of photocatalytic dye degradation on TiO_2 based photocatalysts: A comparative overview. *RSC Adv*. 2014; 4(70): 37003-37026.
43. Nakata K, Fujishima A. TiO 2 photocatalysis: Design and applications. *J Photochem Photobiol C Photochem Rev*. 2012; 13(3): 169-189.

Chapter 3: Methodology

3.1 Synthesis method

3.1.1 Materials

Titanium tetrachloride ($TiCl_4$) 99% and Degussa P25 (80 % rutile, 20 % anatase) were supplied by Sigma Aldrich, South Africa and they were used without further purification. Detonation nanodiamonds were sourced from New Metals and Chemicals Corporation (Japan) and they were used without purification or surface modification.

3.1.2 Preparation of RANR TiO_2

A hydrothermal method was used to synthesize the RANR TiO_2. $TiCl_4$ (12 mL) was added dropwise to 160 mL of deionised water in an ice bath, while stirring. The solution was then refluxed for 16 and 24 hours at various temperatures ranging from 50 to 235 °C. The resulting slurry was cooled to room temperature and then centrifuged for 5 minutes. The solid was then washed five times with warm distilled water to remove chloride ions. The synthesized catalyst was air dried overnight.

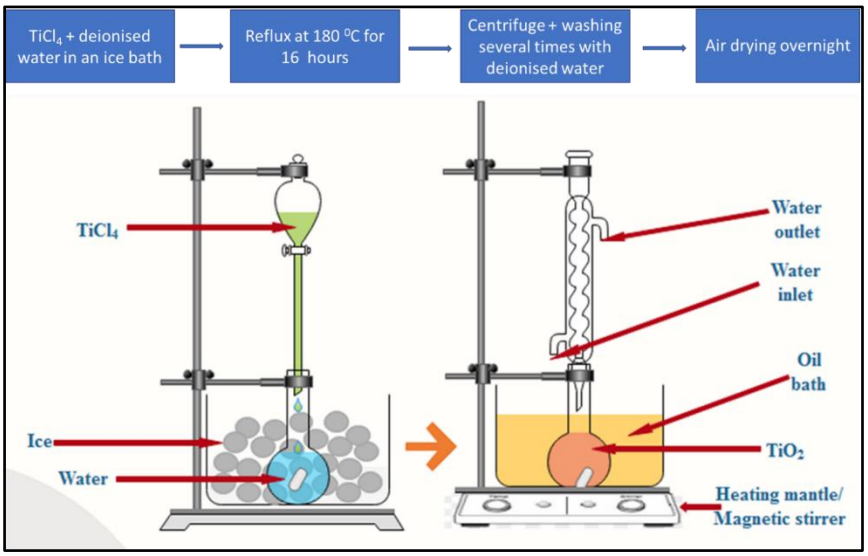

Figure 3.1: Hydrothermal synthesis of TiO_2.

3.1.3 Modification of catalyst

Nanodiamonds were used as the carbon source and the modification was done, in-situ. Different amounts of nano diamonds ranging from 0.1 to 1 weight %, with respect to the mass of RANR TiO_2 were added to water before addition of $TiCl_4$. The solution was then refluxed for 16 hours at 185 °C. The resulting slurry was centrifuged, washed several times with warm distilled water and the catalyst was air dried overnight. Some of the samples were calcined at temperatures between 200 °C and 600 °C to increase the interaction between RANR TiO_2 and nanodiamonds. All the resulting catalysts were characterized to determine the degree of interaction between the RANR TiO_2 and the nano diamonds using characterization techniques listed below.

3.2 Characterization of catalysts

3.2.1 XRD Analysis

XRD was done on the Bruker D2-205530 diffractometer using CuKα radiation (λ = 1.5406 Å) at 30 kV/10 mA which was equipped with a data acquisition computer. All the samples were scanned in the 2θ range between 10° and 90°. PXRD is used to identify phases of a crystalline material and their average crystallite size. The sample to be characterized were crushed into fine powder.

3.2.2 BET Surface area analysis

A Micromeritics RS232 BET surface analyzer was used in this study to measure surface area, pore size and pore volume of the synthesized materials.

3.2.3 SEM Analysis

Scanning Electron Microscopy (SEM) analysis for the synthesized samples was done on a FEI Nova Nano lab 600 SEM. Fine powder samples were placed on a carbon tape and coated using gold (Au) and palladium (Pd) in order to inhibit charging. Energy-Dispersive X-ray (EDX)

spectroscopy connected to the FEI Nova Nano lab 600 SEM was used for elemental analysis. The X-rays were captured using the INCA Microanalysis Suit version 4.08 package software.

3.2.4 TEM Analysis

Solid samples were prepared by sonication in ethanol to disperse the samples for TEM analysis. A drop of the solution was added to a carbon coated copper grid and dried in air before analysis using the FEI Technai T12 TEM with an accelerating voltage of 120 kV.

3.2.5 UV-Vis analysis

A Varian UV-Vis Spectrophotometer was used to determine the concentration of methyl violet dye samples using a beam with a wavelength range between 190 nm and 800 nm.

3.2.6 FTIR Analysis

A Bruker Tensor 27 FTIR analyzer was used for FTIR analysis. Bruker Senterra Laser Raman fitted with a 50x objective lens for imaging and an excitation wavelength of 532 nm was used in this study.

3.2.7 TGA Analysis

TGA analysis was done on a Perkin Elmer TGA Simultaneous analyzer STA 6000 Pyris Series with temperatures of up to 900 $^{\circ}$C. A Perkin Elmer STA 4000 analyzer was used for sample analysis using a flow rate of 10 mL/min, heating rate of 10 $^{\circ}$C/min and 10 mg samples.

3.2.8 XPS Analysis

A Thermo ECSAlab250Xi was used for XPS analysis with monochromatic Al kα x-rays (1 486,7 eV), power of 300 W, x-ray spot-size of 900 μm and pressure less than 10^{-8} mBar.

3.3 Catalytic activities in methyl orange degradation

The synthesized catalysts were applied in photocatalytic organic dye degradation (methyl violet). The degradation efficiency of the composites was determined using 10 mg catalyst, 50 mL of 50 ppm methyl violet for 140 minutes and a comparison was made with pure RANR TiO_2. The catalyst was added to the dye solution which was stirred continuously for 2 minutes in a dark room to homogenize the solution. Aliquots of the solution were taken every 20

minutes, after illumination by a solar simulator, using a 5 mL syringe attached to a 0.45 μm filter to filter off the catalysts. All the aliquots were analyzed by UV-Vis to determine methyl violet concentration.

A Newport solar simulator was used as the light source and the dye solution with the catalyst solution was placed in a quartz reactor. The instrument was set to provide light energy equivalent to the sun. The experiments were all run in a dark room to make sure all the light utilized was from the instrument only. A solar simulator is an instrument that provides illumination in a confined space approximate to that from the natural sunlight. It comprises of a light source, power supply and optical filters which modify the output beam. The light source used was a xenon arc lamp.

3.3.1 Effect of increase in methyl violet concentration

The effect of an increase in methyl violet concentration from 5 ppm to 40 ppm was studied using 10 mg RANR TiO_2 and 50 mL of the dye for 60 minutes. The catalyst (10 mg) was added to the 5 ppm dye solution and was stirred continuously for 2 minutes in a dark room to homogenize the solution. Aliquots of the solution were taken every 10 minutes, after illumination by a solar simulator, using a 5 mL syringe attached to a 0.45 μm filter to filter off the catalysts. All the aliquots were analyzed by UV-Vis to determine methyl violet concentration. Similarly, all the other dye solutions, i.e. 10 ppm, 20 ppm and 40 ppm were studied.

3.3.2 Effect of mass of photocatalyst

A study of the effect of an increase in mass of photocatalyst (5 mg to 40 mg) on the degradation efficiency was done using RANR TiO_2 and 50 mL of 10 ppm methyl violet. The catalyst (5 mg) was added to 50 mL of 50 ppm dye solution and was stirred continuously for 2 minutes in a dark room to homogenize the solution. Aliquots of the solution were taken every 20 minutes,

after illumination by a solar simulator, using a 5 mL syringe attached to a 0.45 μm filter to filter off the catalysts. All the aliquots were analyzed by UV-Vis to determine methyl violet concentration. The same method was used for the other catalyst with different weight, i.e. 10 mg, 20 mg and 40 mg.

3.3.3 Reproducibility studies

Recyclability of the catalyst through 3 cycles was also done using 10 ppm methyl violet and 10 mg of RANR TiO_2. The catalyst was added to 50 mL of 10 ppm dye solution and this was stirred continuously for 2 minutes in a dark room to homogenize the solution. Aliquots of the solution were taken every 10 minutes, after illumination by a solar simulator, using a 5 mL syringe attached to a 0.45 μm filter to filter off the catalysts. All the aliquots were analyzed by UV-Vis to determine methyl violet concentration. The remaining solution was centrifuged and the catalyst was washed with distilled water and re-used in the next cycle.

Chapter 4: Results and discussion

4.1 Characterization of TiO_2

Batches of TiO_2 were synthesized by varying reaction temperatures during refluxing from 50 °C and 235 °C. Fully formed and dense dandelion-like TiO_2 was formed at 180 °C. Refluxing time was interchanged between 16 hours and 24 hours in the current study in order to determine the optimum synthesis parameters of the dandelion-like TiO_2. Aliquots were drawn at 4-hour intervals in order to determine the growth pattern of the RANR TiO_2. From the TEM results obtained, it was observed that RANR TiO_2 was completely formed after 16 hours synthesis time hence there was no need to continue the reaction up to 24 hours. All the other experiments were run for only 16 hours. Several reaction times were recorded in literature ranging from 4 hours [5,1] to 24 hours [2,3]. The differences in the reflux times from the ones recorded in literature can be attributed to the slight variations in the reaction set ups, reaction conditions as well as the different sources of titania used.

4.1.1 Powder X-ray diffraction

All the synthesized catalysts were characterized using XRD, this helped to determine the phases of the TiO_2. Figure 4.1 shows the XRD results for the synthesized catalysts and the commercial Degussa P25. Diffraction angles of 26°, 36°, 38°, 42°, 54°, 56°, 63°, 64°, 69°, 70° all correspond to the (110), (101), (200), (111), (211), (220), (002), (310), (310) and (112) reflections respectively, which show the presence of rutile TiO_2. Reference card numbers used to match peaks are shown in Fig. 4.1. At synthesis temperatures below 200 °C, all the catalysts were pure rutile. A mixture of rutile and anatase starts to format synthesis temperatures above 200 °C. The diffraction angles 23°, 48°, 75° and 86° all belong to anatase and they were present in the commercially available Degussa P25 and other catalysts synthesized above 200 °C. No

characteristic peaks for impurities were detected. The sharp peaks for P25 suggest that P25 was more crystalline than the synthesized TiO_2[1]. TiO_2 synthesized at 180 °C had a sharper and narrower peak (at 26°) as compared to the rest of the synthesized TiO_2, which suggests that fully formed dandelions show enhanced crystallinity and growth[6].

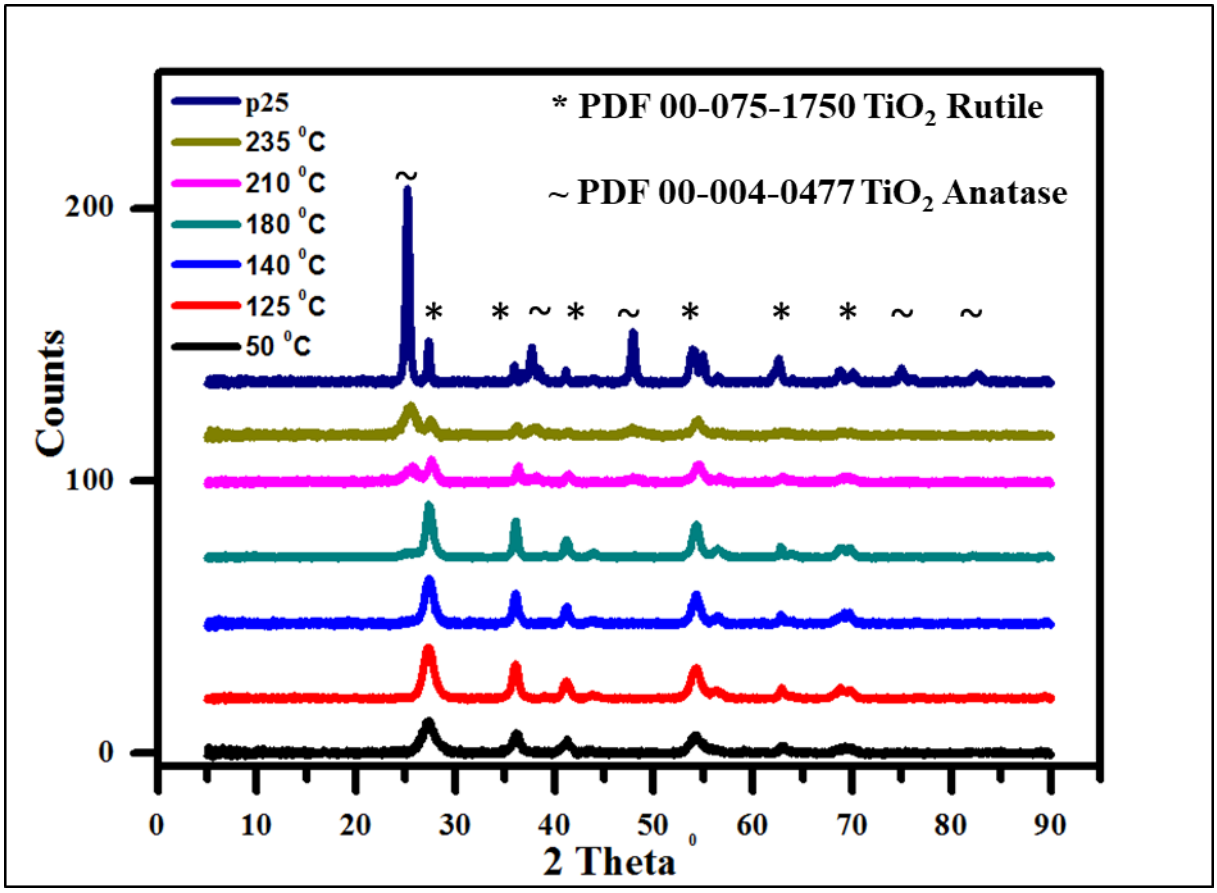

Figure 4.1: XRD patterns for rutile TiO_2 synthesized at different temperatures (°C) compared to p25.

4.1.2 Microscopy Analysis (TEM and SEM)

The growth mechanism of the RANR TiO_2 was determined by sampling 30 ml aliquots during reflux every 4 hours of the reaction. TEM images showed that nucleation, then growth was responsible for the formation of the dandelion-like TiO_2. At the start of the reaction between $TiCl_4$ and H_2O, TiO_2 nuclei are formed. The TiO_2 nuclei are shown as the small dots (pointed by the red arrows) in the images in Figure 4.2a and 4.2b at 4 hours and 8 hours respectively. The TiO_2 nuclei then aggregate and grow to form rods which then grow and self-assemble as

shown in Figure 4.2c (12 hours) or self-align radially forming half-dandelions, which then fully grow to become dense dandelion-like structures (Figure 4.2 d).

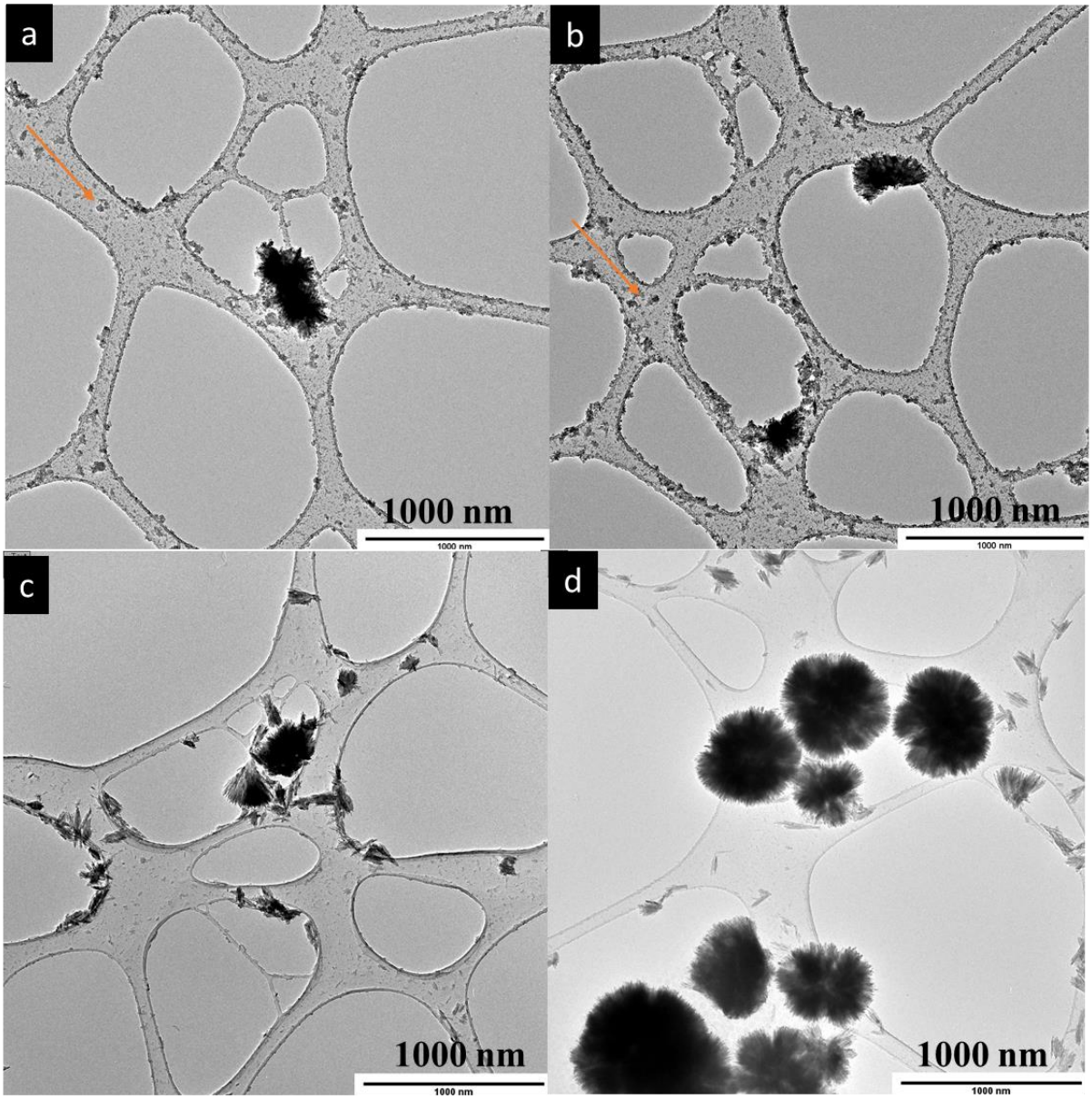

Figure 4.2: TEM images for aliquots sampled after 4 hours (a), 8 hours (b), 12 hours (c) and 16 hours (d) synthesized at 180 °C.

Figure 4.3 shows the proposed mechanism highlighting nucleation of TiO_2, formation and growth of nanorods. This is then followed by self-alignment of the nanorods, until a full dandelion structure is formed. Reflux temperature and reaction time were the main parameters that affected the growth pattern of the RANR TiO_2. A nucleation and nuclei growth-dissolution-recrystallization growth mechanism was proposed in a similar study where

nucleation first occurred to form TiO_2 islands, followed by growth of nanowires to finally give RANR TiO_2. Jin Yi et.al also suggested a similar mechanism, except that they used SnO_2 spheres. TiO_2 crystal nuclei formed on the surface of the spheres, then nanorods grew towards the centre forming the dandelion-like structure, thereby dissolving the SnO_2[5].

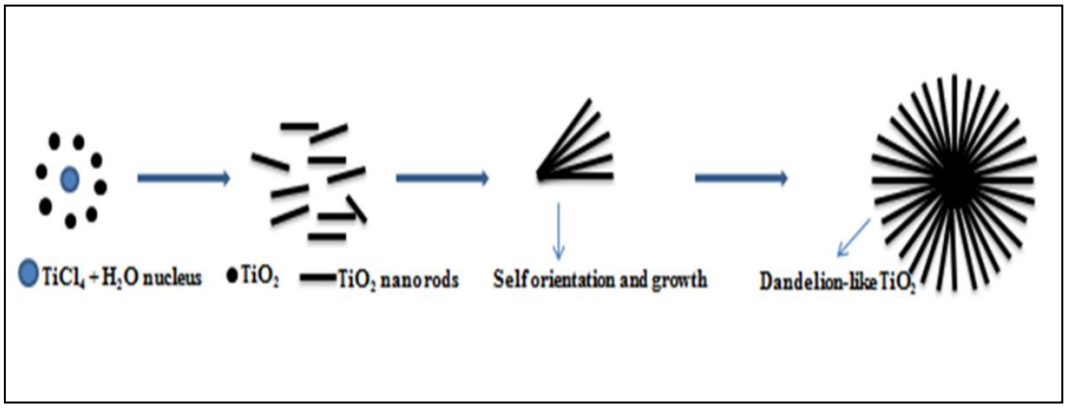

Figure 4.3: The proposed mechanism for RANR TiO_2 formation at a reflux temperature of 180 °C and reflux time of 16 hours.

The effect of reaction temperature on the morphology of TiO_2 was also studied. TEM images obtained for reaction temperatures lower than 140 ^{0}C show that the rods will be self-aligning radially (Figure 4.4a and b) and at 140 ^{0}C (Figure 4.4c), they form structures which are almost complete dandelions, but the rods are loosely packed. The increase in synthesis temperature to 180 ^{0}C leads to the formation of fully-formed dandelion-like structures, which are densely packed (Figure 4.4d). At temperatures above 200 ^{0}C, the dandelion-like shape is lost, as shown in Figure 4.4(e) and (f). Loosely packed nanorods were synthesized by Xuelian et al. at 160 ^{0}C whereas dense, compact dandelion-like structures were synthesized using a temperature range of between 180 ˚C and 190 ˚C [1]. It was also reported temperature was an important factor in the synthesis of RANR TiO_2, 80 ˚C yielded loosely packed nanorods, 100 ˚C led to the formation of perfect RANR whereas temperatures as high as 190 ˚C destroyed the dandelion-like structure of TiO_2[2].

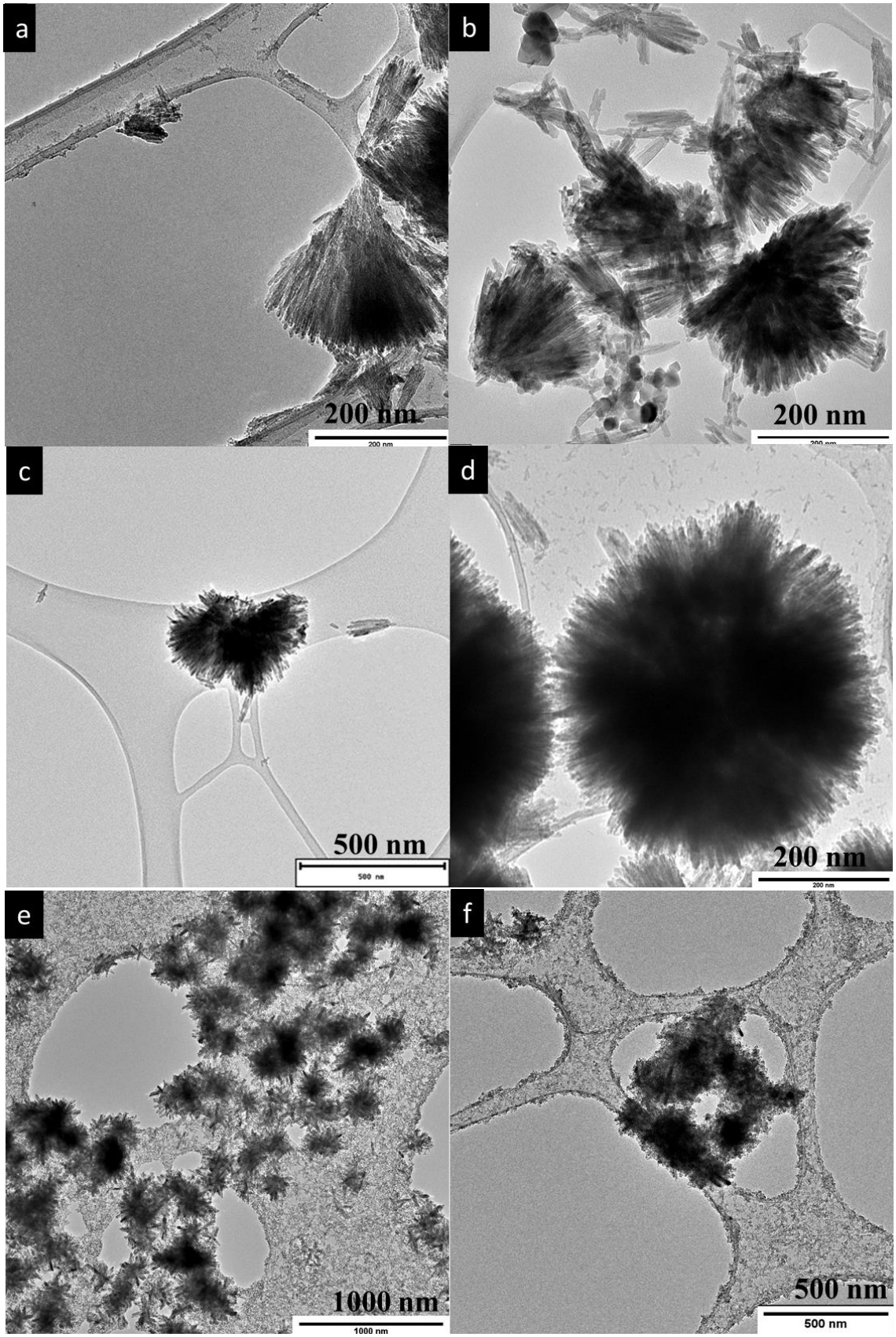

Figure 4.4: TEM images for dandelions synthesized at 50 °C (a), 125 °C (b), 140 °C (c), 180 °C (d), 210 °C (e) and 235 °C (f).

SEM was also used to confirm the morphology of the TiO_2. This characterization technique was also important to show the 3-dimensional structure of the dandelion-like morphology of the RANR TiO_2. The RANR TiO_2 were pictured as densely packed spheres with different sizes as shown in Figure 4.5 below.

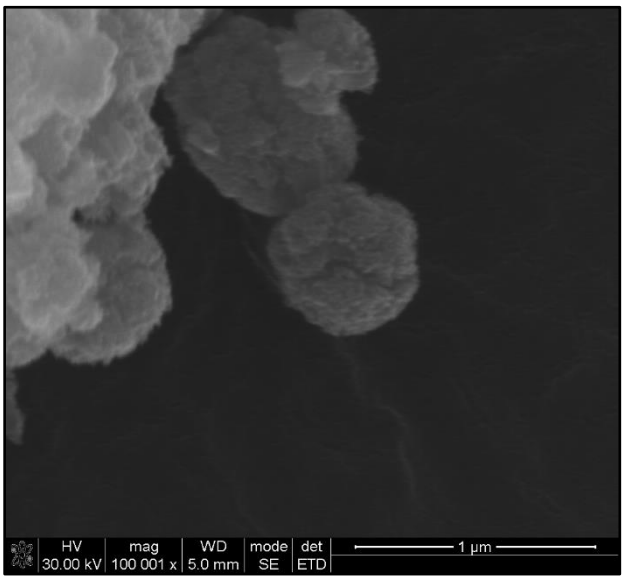

Figure 4.5: Figure showing synthesized dandelions at 180 °C for 16 hours

The synthesized RANR TiO_2 had a wide size distribution range, ranging from 300 nm to 800 nm. The size of the dandelions is mostly affected by the synthesis method and synthesis temperature. The average size of the dandelion-like TiO_2 was 530 ± 65.4 nm. The TEM images in Figure 4.6 below show the dandelions with different sizes.

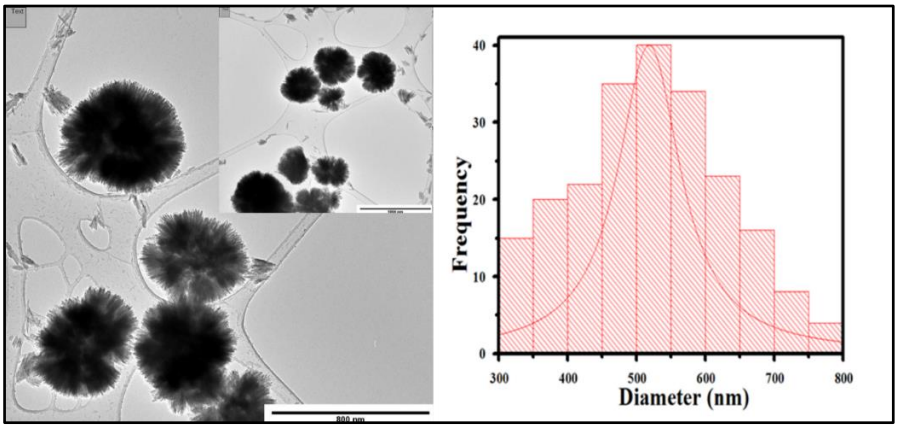

Figure 4.6: TEM micrograph and insert showing dandelions of different sizes (left) and a graph showing particle size distribution (right).

SEM with EDS was used for elemental analysis of the synthesized catalysts (Figure 4.7). Gold and palladium were used to coat the samples to inhibit charging. Traces of chlorine (less than 0.5%) were also present in all the samples originating from the titanium precursor ($TiCl_4$). All the samples were washed several times with warm distilled water after centrifuging in order to get rid of chloride ions but the chloride was still present in trace amounts. The presence of trace amounts of chloride was also confirmed by XPS analysis.

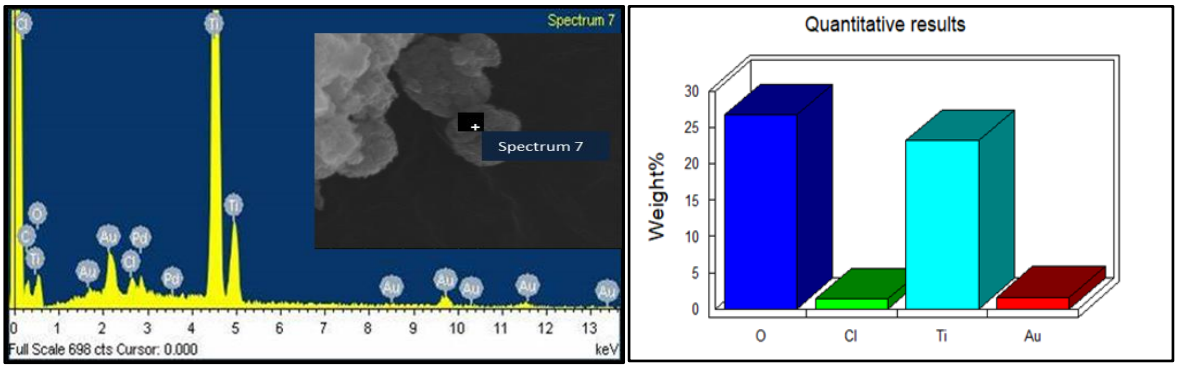

Figure 4.7: SEM with EDS plot and quantitative results for the synthesized dandelions.

4.1.3 BET Surface Area Analysis

BET Surface area analysis was used to determine the surface areas of the synthesized catalysts. The trend in surface areas corresponds to the TEM images obtained. All the synthesized photo catalyst had high surface areas as compared to the commercially available catalyst (Degussa P25). There was a decrease in surface area with increase in synthesis temperatures from 50 °C to 180 °C. At low temperatures, the nano rods are small and still growing, hence the high surface area. Above 50 °C, the rods continue to grow thereby decreasing surface area until at 180 °C, where they are fully grown to form complete dandelion structures. At temperatures above 200 °C, the nano rods disintegrate to smaller particles, which results in the sudden

increase in surface area. Table 4.1 shows the BET surface areas. The BET surface areas for RANR in similar studies are shown in the table. The differences can be attributed to the variations in synthesis temperatures of the dandelion-like TiO_2.

Table 4.1: Table showing BET surface areas of the synthesized TiO_2 catalysts

Sample	BET Surface area (m^2g^{-1})	Pore size (nm)	References
P25	**45**	**6.5**	**This current project**
TiO_2 (50 °C)	**164**	**2.5**	
TiO_2 (125 °C)	**83**	**4.0**	
TiO_2 (140 °C)	**81**	**4.0**	
TiO_2 (180 °C)	**68**	**4.3**	
TiO_2 (210 °C)	**142**	**3.2**	
TiO_2 (235 °C)	**148**	**2.5**	
Dandelions (100 °C)	**81**	**3.2**	[7]
Dandelions (120 °C)	**40**	**–**	[6]
Dandelions (180 °C)	**46**	**–**	[5]

4.1.4 Solid State UV-Vis Analysis

Solid state UV-Vis analysis showed that all the photocatalysts absorbed light in the UV region (350 nm) with almost the same absorption trend as shown in Figure 4.8. Another small peak was also present in the visible region at around 530 nm as shown in Figure 4.8 which means

that the photocatalysts absorb some light in the visible range. The high absorbance in p25, TiO_2 synthesized at 180 °C and 125 °C is attributed to the increase in crystallinity as shown in the sharp XRD peaks (Fig. 4.1). The lower absorbance in RANR 210 °C, 235 °C and 50 °C is also attributed to the decreased crystallinity which is also shown by XRD peaks. Band gap energies were calculated using a Tauc's plot (Figure 4.9). Fitting absorption data to equations for both direct and indirect bandgap transitions is a method that is used to determine band to band transitions in a material[8]. A graph of $(\alpha hv)^2$ vs Eg is used for direct transitions, $\alpha^{1/2}$ vs Eg for indirect transitions, where α is the absorption coefficient, Eg is the band gap energy and hv is photon energy. The value of hv extrapolated when α is 0 gives an absorption energy equivalent to the bandgap energy (Eg)[8].

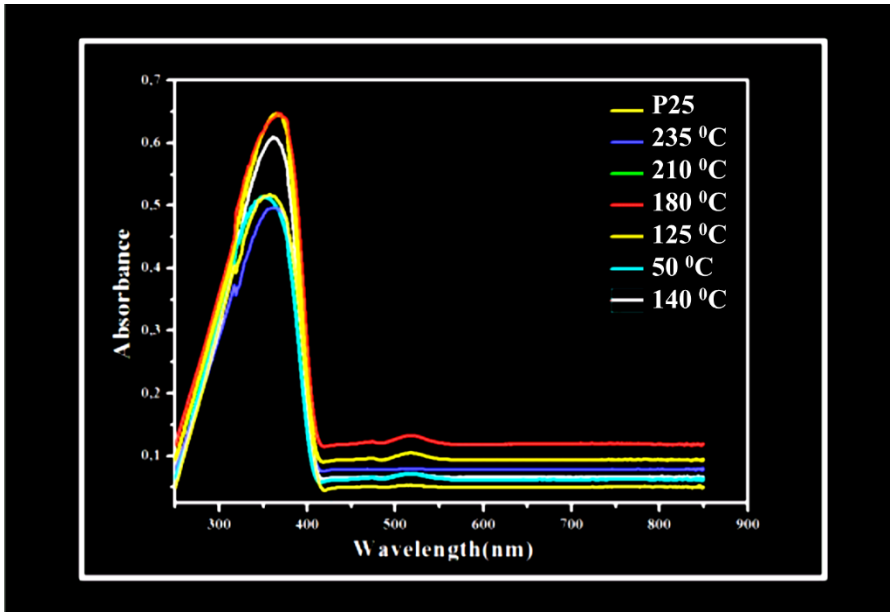

Figure 4.8: UV-Vis graph showing effect of synthesis temperature on absorbance.

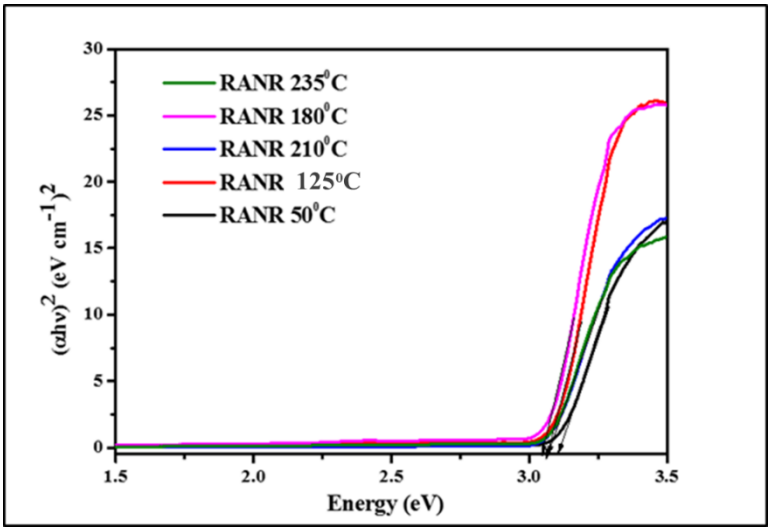

Figure 4.9: Graph showing band gap calculations using Tauc plot.

All the synthesized catalysts absorption data fit the equations for direct band gap transitions (Table 4.2). The direct band gap decreased as synthesis temperature increased up to 180 °C and then started increasing with the increase in temperature to 235 °C. The fully formed dandelions (180 °C) had the least band gap energy.

Table 4.2: Band gap energies

Sample	Bandgap Energy (Ev)
RANR TiO_2 50 °C	**3.1**
RANR TiO_2 125 °C	**3.06**
RANR TiO_2 180 °C	**3.04**
RANR TiO_2 210 °C	**3.07**
RANR TiO_2 235 °C	**3.08**

4.2 Characterization of nanodiamonds

The nanodiamond samples were obtained as a waste material from the detonation of carbon-containing explosives (detonation nanodiamonds). Characterization was necessary to confirm the presence of diamond grains in the sample and to determine their size, surface composition and surface area.

4.2.1 PXRD Analysis of nanodiamonds sample

The diffraction angles (2Θ) of 44°and 75.5° from the XRD pattern in Figure 4.10 correspond to the (111) and (220) reflections of diamond which shows the presence of diamond grains in the sample[9]. The length of nanodiamonds grain in the (hkl) direction was determined using the Scherrer formula ($L_{hkl} = k\lambda/\beta_{hkl}\ Cos\Theta_{hkl}$), where λ is the wavelength used, β_{hkl} is the Full width half maximum of x-ray diffraction hkl, Θ_{hkl} is the angle corresponding to the peak and k is a constant[10]. The length of nanodiamonds in the (111) direction is 3.6nm, which is in the range of 2-10 nm[11] as other calculated values in literature 3.8 nm[10], 5 nm[12].

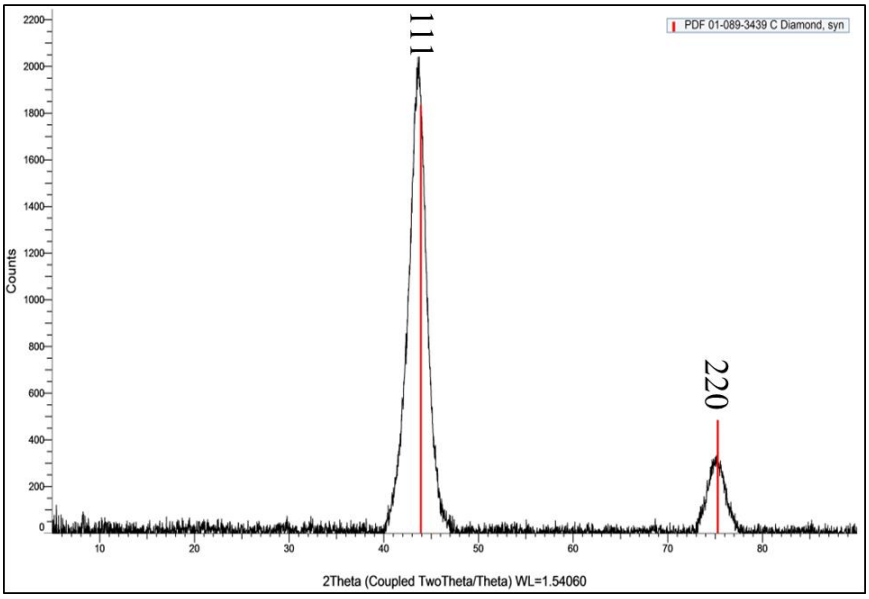

Figure 4.10: XRD graph for the nanodiamonds sample.

4.2.2 Microscopy Analysis

The TEM images in Figure 4.11 shows the presence of nanodiamond particles with sizes less than 10 nm. The nanodiamonds in the TEM images appeared to be either spherical or elliptical as shown in Fig. 4.11a and b.

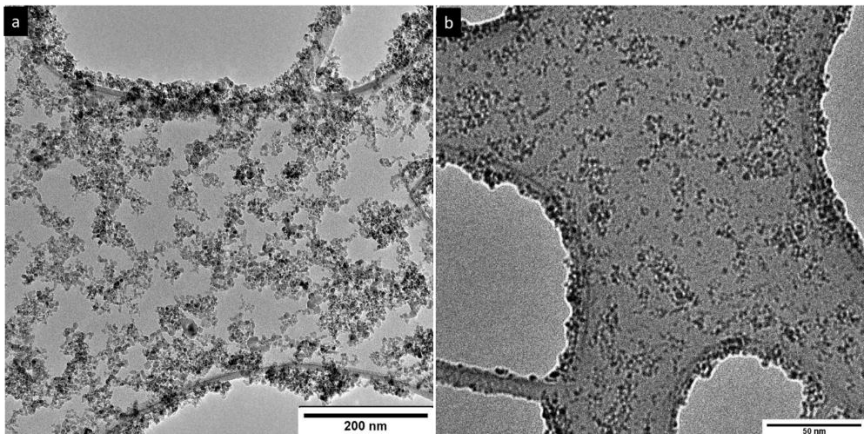

Figure 4.11: TEM images for the detonation nanodiamonds at 200 nm (a) and 50 nm (b).

4.2.3 Raman Spectroscopic Analysis

There was background fluorescence in the RAMAN spectrum and after background subtraction, the spectrum was still noisy due to the signal to noise ratio from the fluorescence. The Gaussian and Lorentzian functions were used to show the presence of overlapping peaks (Figure 4.12). The fluorescence was due to nitrogen vacant centres, as nitrogen is a common impurity in nanodiamonds[13,14].

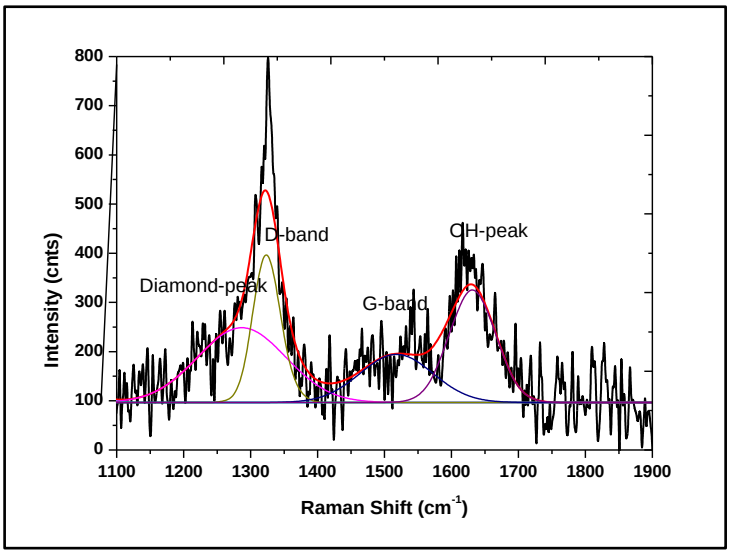

Figure 4.12: Raman spectra of the nano diamonds sample

The presence of nitrogen in the nanodiamonds was confirmed by XPS. The peak at 1290 cm^{-1} corresponds to diamond (sp^3 hybridized carbon), but it shifted from 1330 cm^{-1}, due to residual stress in the material. It is also broad, which shows that the nanodiamonds were deformed plastically and they have poor crystal quality. The peak at 1633.8 cm^{-1} corresponds to sp^2 hybridized carbon, which is present on the nanodiamonds outer shells. D and G bands of sp^2 (graphitic carbon) present, explain the opaque grey colour of the sample. The mixture of sp^2 and sp^3 hybridized carbon confirms the presence of nanodiamonds since they have a diamond core with a graphitic shell[10,13].

4.2.4 FTIR Analysis

FTIR analysis was done to determine the functional groups present on the graphitic (sp^2) carbon outer shell of the nanodiamonds. FTIR is a highly sensitive method for the determination of the surface chemistry of nanodiamonds[24], however, the presence of the diamond core can be confirmed using Raman spectroscopy. The functional groups present originated from the detonation of carbon-containing explosives, the type of the functional groups present highly depends type of explosives used and the nanodiamonds purification process. In this study, the

nanodiamonds used were not purified since the functional groups were required to increase the interaction with TiO_2. FTIR results in Figure 4.13 show the presence of -OH stretching and H_2O bending vibrations at 3410 cm^{-1} and 1605 cm^{-1} respectively which is evidence that the graphitic layer of the nanodiamonds (neighbouring carboxylic groups) adsorbed moisture from the environment. This is evidenced by the drastic -OH and H_2O peak reduction after annealing in Fig. 4.20

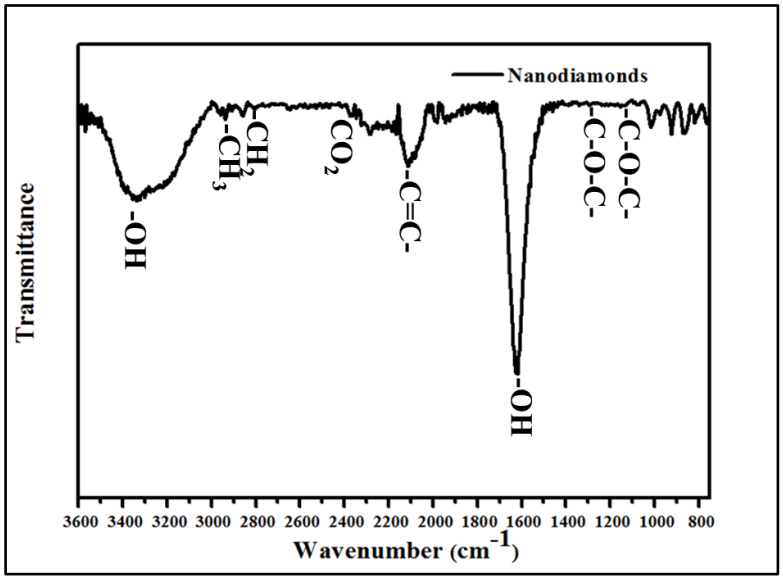

Figure 4.13: FTIR graph for nanodiamonds.

The peaks at 2850 cm^{-1} and 2955 cm^{-1} are due to the presence of stretch vibrations of the $-CH_2$ and $-CH_3$ absorptions. The peak at 2340 cm^{-1} is due to the presence of CO_2 absorptions. The peaks at 1260 cm^{-1} and 1120 cm^{-1} are due to the presence of -C-O-C groups on the surface. The functional groups present in the sample were -OH, CO_2, CH_2, CH_3, C=C, -C-O-C among others. The sp^2 hybridized carbon on the surface of nanodiamonds in a similar study were functionalised with C=O, C-O and C-OH groups among others[15]. The nanodiamond surface characterised by Q. Zou et.al. also showed the presence of functional groups such as the OH, H_2O, CH_3, CH_2, COOH, C=O, CO_2 and -C-O-C-[10].

4.3 Characterization of RANR TiO_2-Nanodiamond composite

Composite samples were synthesized in situ with 0.1, 0.5 and 1 weight % of nano diamonds. The samples were calcined at 200 °C, 400 °C and 600 °C for 3 hours with a heating rate of approximately, 4 degrees/min. Calcination was done in an attempt to increase the interaction of the nanodiamonds with TiO_2 and to also increase crystallinity of the composite. Calcination temperatures were kept at 200 °C for the rest of the composites (0.1, 0.5 and 1 weight %), since higher temperatures destroyed the dandelion-like structure of RANR TiO_2.

4.3.1 TEM Analysis

TEM images show that the nanodiamonds were located on the tips of the nanorods, surrounding the RANR TiO_2 in TND 0.1% (Figure 4.15(a)). Increase in the nanodiamond loading from 0.1% to 1% showed that only a few nanodiamonds were surrounding the tips of the nanorods, whereas the rest were not attached to the nanorods as shown in Figure 4.15(c) and 4.15(e). Modification of the RANR TiO_2 with nanodiamonds disrupted the nanorod structure (in Figure 4.15(a), 4.15(c) and 4.15(e)). Nanorods were regenerated by calcination, increasing the crystallinity of the RANR TiO_2, which is shown by the increase in intensity of the Eg peak in Raman analysis. Calcination at 200 °C helped to increase the interaction between the RANR TiO_2 and the nanodiamonds since more distinct dandelions were formed as shown in Figure 4.15(b), 4.15(d) and 4.15(f).

Calcination of the composites at high temperatures above 200 °C led to the loss of the nanorod morphology, giving rise to a more uniform phase, which resembled spheres, as seen in Figure 4.15(g) and (h). Calcination of the materials led to the formation of more uniform morphologies, as shown in Figure 4.15(b), (d), (f), (g) and (h), but BET surface area analysis (Table 4.3) showed a drastic decrease in surface area with calcination, due to the collapse of

pores. High temperatures above 600 °C could not be used, since TGA analysis showed that nanodiamonds start to decompose above 600 °C.

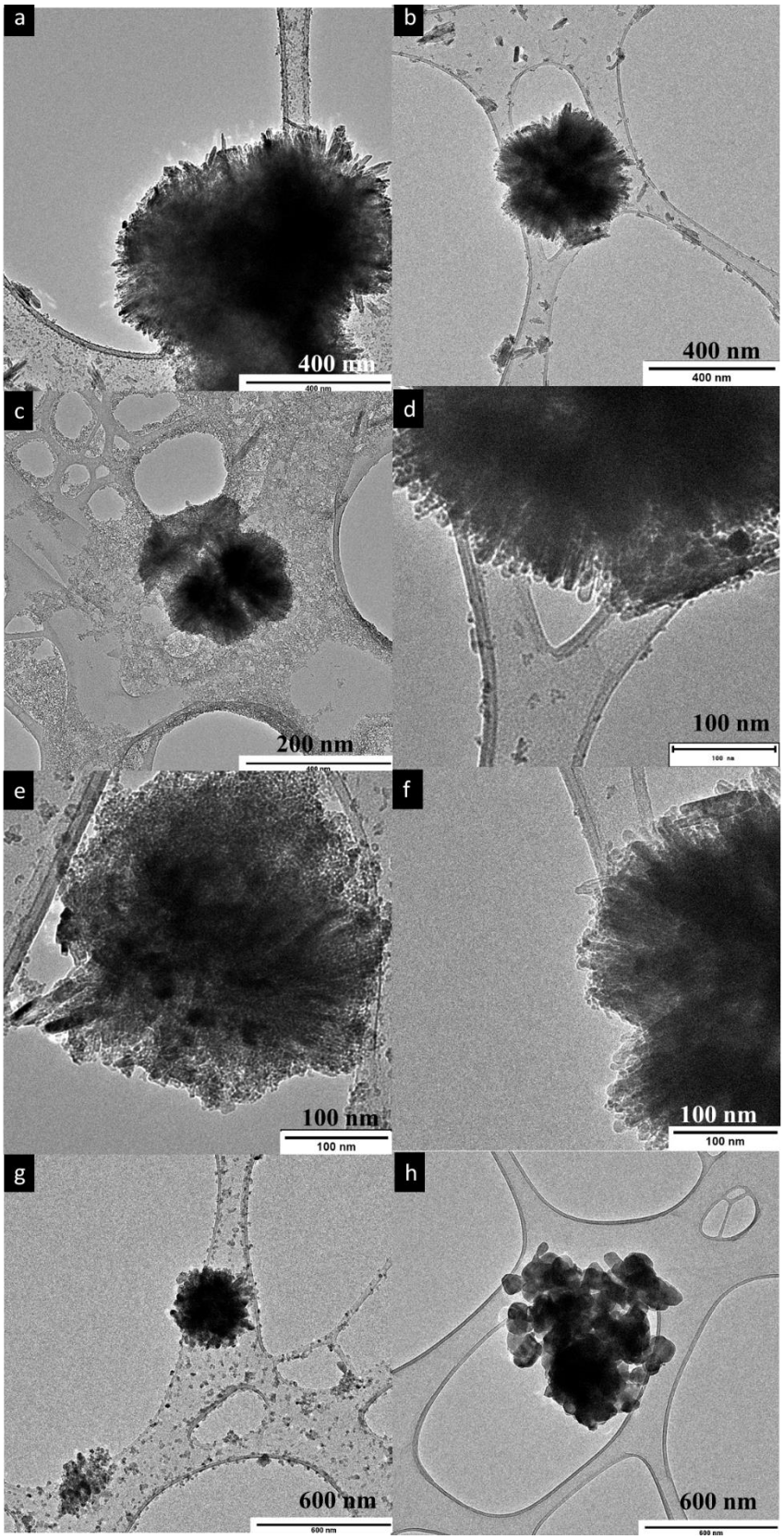

Figure 4.14: TEM images showing TiO_2- nano diamonds samples (a) TND 0.1%, (b) TND 0.1% calcined at 200 °C, (c) TND 0.5%, (d) TND 0.5 % calcined at 200 °C, (e) TND 1%, (f) TND 1% calcined at 200 °C, (g) TND 0.1% calcined at 400 °C and (h) TND 0.5% calcined at 200 °C.

4.3.2 BET Surface Area Analysis

BET Surface area analysis showed that modification of the RANR TiO_2 with nanodiamonds led to a significant increase in surface area, from 68 m^2/g to 83 m^2/g for the composite with 0.1 % loading as shown in Table 4.3. The surface area further increased to 107 m^2/g and 156 m^2/g with an increase in nanodiamonds content of 0.5 and 1 % ,respectively, since the nanodiamonds have high surface areas of 244 m^2/g. The composite sample with the highest nanodiamond loading (TND 1%) had the highest surface area because an increase in nanodiamond loading also increased the amount of unattached nanodiamonds. The surface areas of the composites were lower than the nominal value obtained by the finding the average of the surface areas of the RANR TiO_2 and the nanodiamonds. This discrepancy is evidence of contact between the surface of TiO_2 nanodiamond phases or it could be due to the formation of larger TiO_2 particles during composite synthesis[12]. As surface area was increasing, the pore size was also decreasing. Calcination led to a significant decrease in surface area of all the composites, this can be attributed to the collapse of pores in the TiO_2[12].

Table 4.3: BET surface area analysis of the composites

Material	BET surface area (m^2/g)	Pore size (nm)
RANR TiO_2 (dandelions)	**68**	**4.3**
Nanodiamonds	**244**	**3.2**

TND 0.1%	**83**	**3.8**
TND 0.5%	**107**	**3.6**
TND 1%	**156**	**3.5**
TND 0.1%, 200 °C	**64**	**3.3**
TND 0.5%, 200 °C	**76**	**3.1**
TND 1%, 200 °C	**120**	**3.0**

4.3.3 Raman Spectroscopic Analysis

The band at 230 cm^{-1} in the RAMAN spectra (Figure 4.16) is due to disorder induced scattering or second-order effect which results from multi-phonon processes[16].

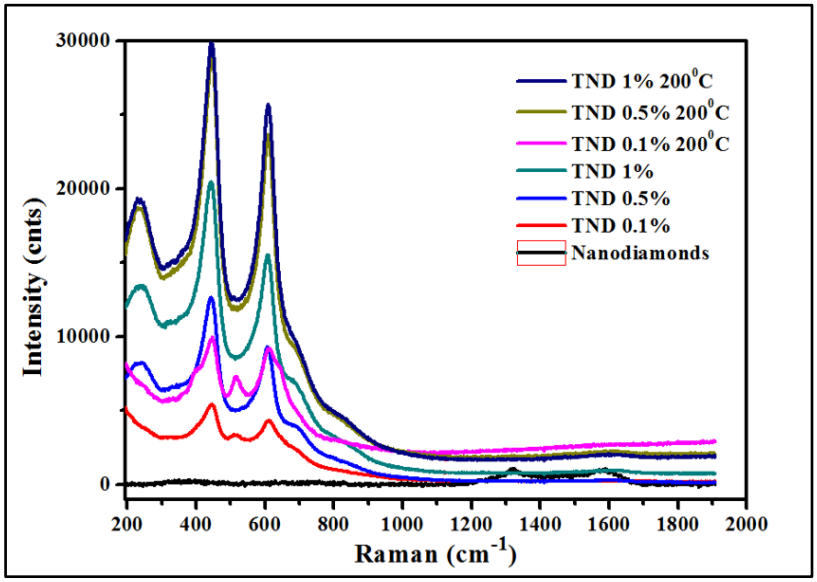

Figure 4.15: Raman graph showing the TiO_2-nanodiamond composites.

The bands at 440 cm^{-1} and 600 cm^{-1} are due to E_g and A_{1g} phonons of Raman active single crystalline rutile. The increase in intensity of the E_g peak (440 cm^{-1}) can be attributed to the increase in crystallinity of TiO_2 after calcination[16]. The band at 1600 cm^{-1} in the composite can be attributed to sp^2 hybridized carbon[17]. The nanodiamonds were dispersed in all the samples,

because low percentage loadings were used for synthesis or they were coated by the dandelions. There is a peak at around 1640 cm^{-1} in TND samples (Figure 4.17) which can be attributed to sp^2 hybridized carbon in the nanodiamonds, but it broadened and shifted from 1590cm^{-1} due to residual stress in the material and deformation which could have been due to the interaction of carbon with TiO_2 or due to the formation of new bonds between carbon and titanium[13;18].

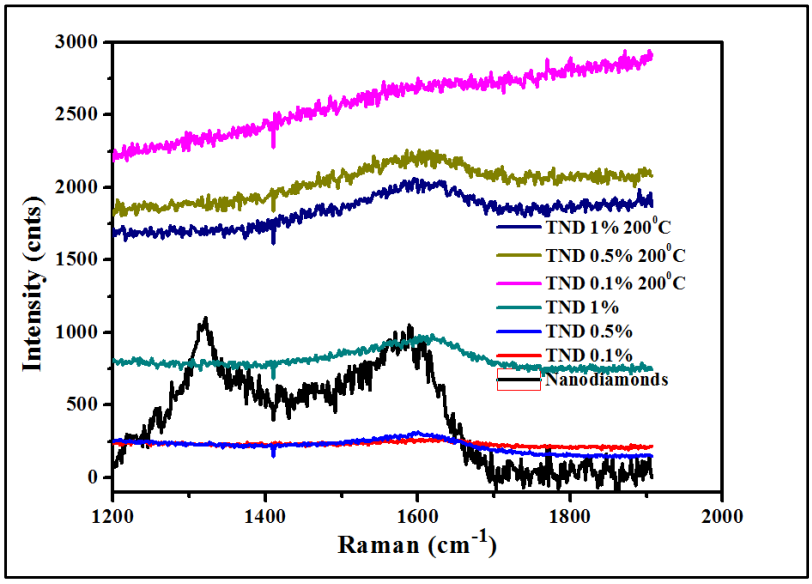

Figure 4.16: Raman graph (same as Fig. 4.16 above) showing the presence of sp^3 hybridized carbon in a TiO_2-nanodiamond composite samples.

4.3.4 Solid State UV-Vis Analysis

Solid state UV-Vis data (Figure 4.18) showed that the dandelions and TiO_2-nanodiamond samples all absorbed light at the same wavelengths (350 nm and 530 nm). There was not much difference in the absorption between pure dandelions and the composites, also, the nanodiamonds did not increase absorbance of light in the visible region as was expected. Uv-vis data was used to determine band gap energies of the materials and to determine the type of transitions in the band gap whether direct or indirect. Fitting absorption data to equations for both direct and indirect bandgap transitions is a method that is used to determine band to band transitions in a material. A graph of $(\alpha h\nu)^2$ vs Eg was used to determine the band gap energies

for direct transitions where α is the absorption coefficient, Eg is the band gap energy and hv is photon energy in Figure 4.19. The value of hv extrapolated to α=0 gives an absorption energy equivalent to the bandgap energy (Eg)[8].

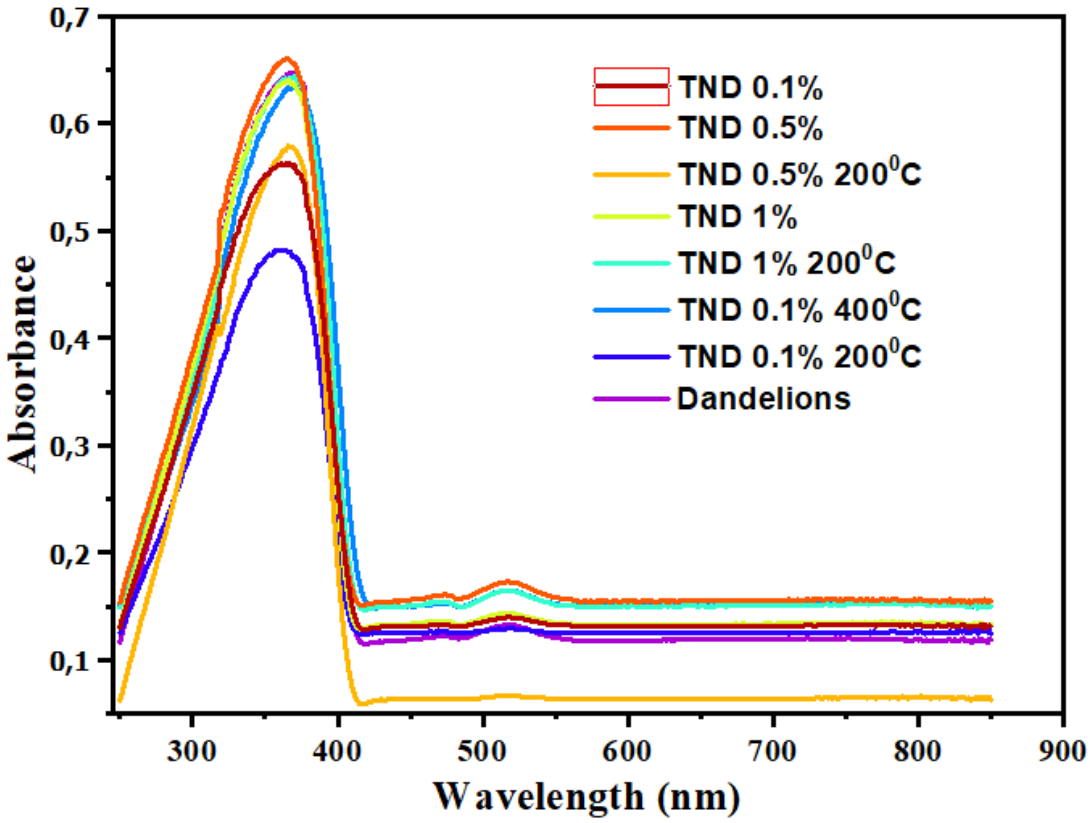

Figure 4.17: UV-Vis spectra of the TiO_2-nanodiamond composites.

The solid-state UV-Vis data obtained for all the composites fit the equation for direct band gap transitions which suggests that they were all direct bandgap semiconductors. Band gap energies increased slightly from 3.04 eV (dandelions) after composite synthesis due to the high band gap energy of nanodiamonds which is approximately 5 eV (Table 4.4). Increasing the nanodiamond weight percentage loading also slightly increased the band gap energies. Calcination led to a decrease in the band gap energies. Electronic transition from the VB to the CB is electron dipole allowed for direct band gap semiconductors, this means that electronic absorption and emission is usually strong which leads to more efficient absorption of solar

energy[8]. Indirect bandgaps on the other hand have phonon assisted transitions because VB to CB transitions are electrical dipole forbidden, both energy and momentum of the electron-hole pair are changed during transmission hence weak absorptions[8].

Table 4.4: Band gap energies for the composites

Sample	Bandgap Energy (eV)
Dandelions	**3.04**
TND 0.1%	**3.05**
TND 0.5%	**3.07**
TND 1%	**3.07**
TND 0.1%, 200 °C	**3.05**
TND 0.5%, 200 °C	**3.06**
TND 1%, 200 °C	**3.04**
TND 0.1%, 400 °C	**3.02**

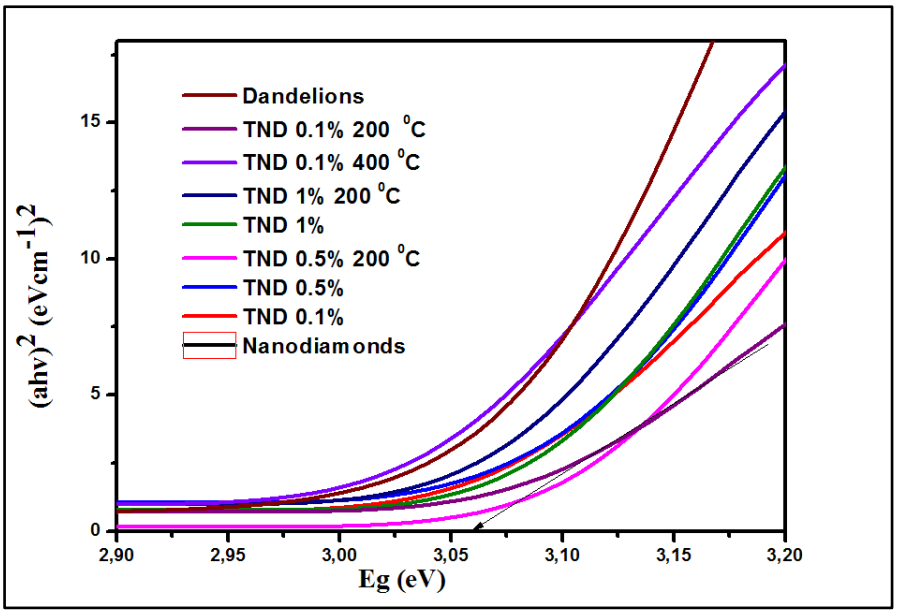

Figure 4.18: Figure showing a Tauc's plot for band gap energy determination

4.3.5 FTIR Analysis

FTIR analysis was done to determine the surface groups present in the TND composite (1 % loading) and to determine if any new bonds were formed during the composite synthesis. FTIR results in Figure 4.20 show the presence of -OH stretching and H_2O bending vibrations in all the samples except the once calcined at 3410 cm^{-1} and 1605 cm^{-1} respectively which is evidence that the nanodiamonds outer shell (adjacent carboxylic groups) adsorbed moisture from the environment. The peaks at 2850 cm^{-1} and 2955 cm^{-1} in nanodiamonds and TND are due to the presence of stretch vibrations of the $-CH_2$ and $-CH_3$ absorptions. The peak at 2340 cm^{-1} is due to the presence of CO_2 absorptions. Peaks at 1400 cm^{-1} and 1290 cm^{-1} (-C-O-C-) became more prominent after the composite synthesis which are evidence of interaction between the RANR TiO_2 and the nanodiamonds. Calcination of the composite removed almost all the moisture due to evaporation.

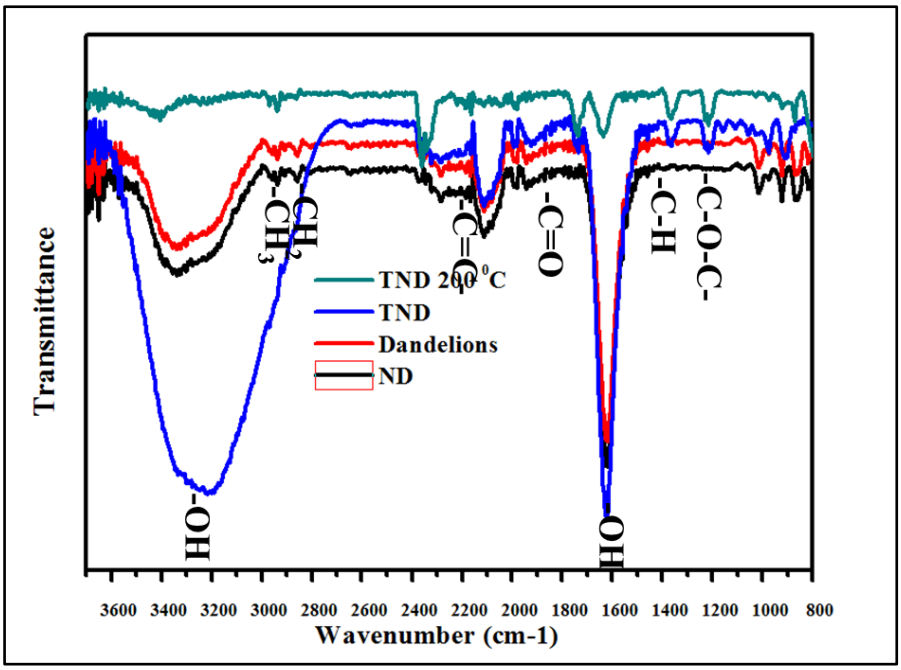

Figure 4.19: FTIR graph for the synthesized catalysts.

4.3.1 XPS Analysis

XPS analysis was used to determine elemental analysis, chemical bonds identification and surface contamination determination on one composite sample that had 1% weight loading of nanodiamonds. The results obtained show that oxygen, carbon, titanium were all present in the sample as shown in Figure 4.21. Two impurities were also present on the surface of the sample which are chlorine and nitrogen with atomic percentages of 1.4 % and 0.4 % respectively. Chlorine (Cl 2p) could have been from the titanium tetrachloride which was used as the titanium source during synthesis. The chlorine was also revealed by SEM with EDS as shown in Figure 4.7. XRD and other characterization techniques did not reveal the presence of chlorine since it is only available in small quantities. Attempts to remove the chloride ions was done by washing the composite with warm distilled but it was not 100% effective. It was also hard to tell if the chlorine was attached to TiO_2 only, or to the nanodiamonds or both since the composite synthesis was done in-situ.

The nitrogen (N 1s) present in the sample was from the detonation nanodiamonds as it is a common impurity. Nitrogen comes from the nitrogen vacant (NV) centres in the nanodiamond core, its presence was also confirmed by the high background fluorescence in Raman analysis (Fig 4.12). Acid purification of nanodiamonds removes metallic impurities and modifies the surface groups on the sp^2 hybridized outer shell carbon[14] not the diamond core. Other methods of purification like the gas phase method[25] and ozone purification[26] only modify or get rid of non-diamond carbonaceous (sp^2) products. In this current project, the nanodiamonds were used as they were without purification in order to increase the interaction of the sp^2 functionalised outer shell with TiO_2.

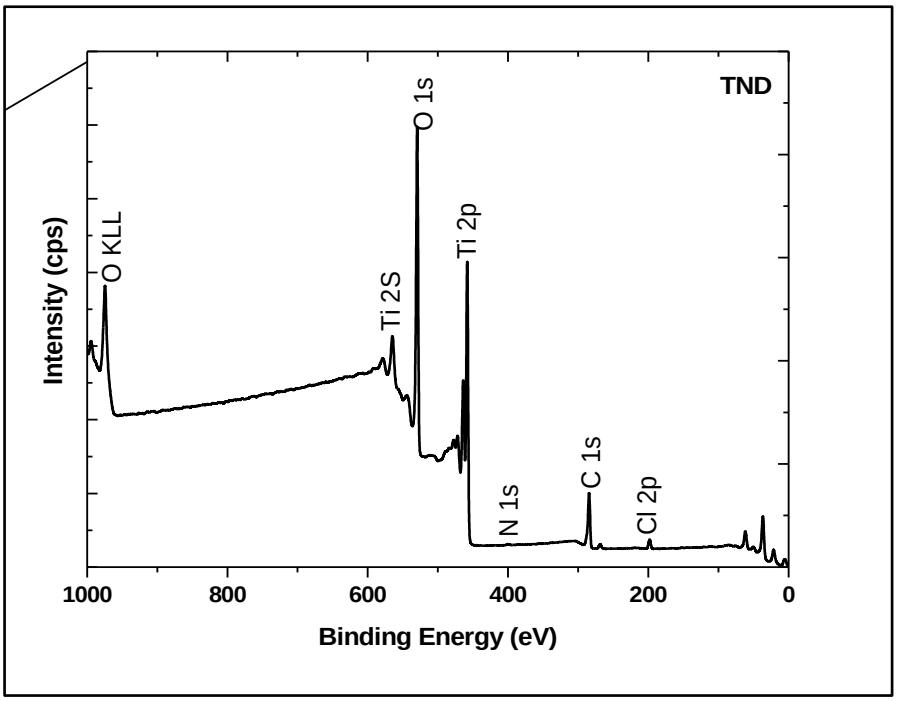

Figure 4.20: XPS survey spectrum for TiO_2-nanodiamond sample with 1% weight loading.

Table 4.5: Elements with their corresponding binding energies and atomic weight percentage

Element	Peak Binding Energy (eV)	Atomic Percentage (%)
O 1s	**529.4**	**50.8**
C 1s	**284.3**	**24.8**
Ti 2p	**458.1**	**22.6**
Cl 2p	**198.1**	**1.4**
N 1s	**399.8**	**0.4**

Gaussian deconvolution was used to show the presence of overlapping peaks and to separate them for easy identification. The additional peaks that were identified are shown in Figure 4.22.

Three types of C 1s atoms were present as shown in Figure 4.22 below, this is supported by the FTIR data. The most abundant one on the surface was from C-C bonds with 20.7 atomic percentage with a peak at 284.4 eV, followed by C-O AT 286.1 eV, then finally O-C=O at 288.4 eV with 3.3 % and 2.6 %, respectively. The C-C bonds on the surface were from the graphitic carbon shell on the nanodiamonds and the C-O bonds can all be attributed to the surface groups on the graphitic carbon shell of the nanodiamonds[19]. There was no evidence suggesting the presence of a Ti-C bond. Hashimoto suggested that a C 1s peak at 281.8 eV can be attributed to a Ti-C bond which is formed by the substitution of some of the lattice oxygen atoms[20].

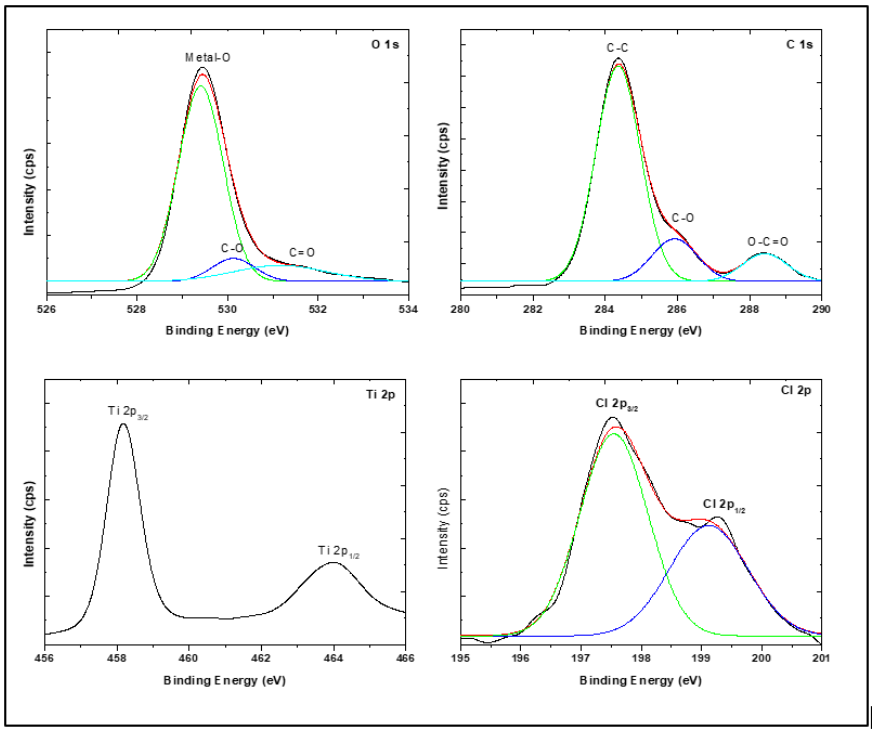

Figure 4.21: XPS high resolution spectra for TiO_2-nanodiamond sample with 1% weight loading showing O 1s, C 1s, Ti 2p, Cl 2p.

The Ti 2p peak at 458.2 eV with 21.6 atomic percentage as shown in Figure 4.22 was due to the presence of Ti $2p_{3/2}$ which is also present in pure rutile TiO_2. The peak at 464.0 eV with

atomic percentage of 1.0 % can be attributed to the presence of Ti $2p_{1/2}$ which is also found in pure rutile titania[19]. There was no evidence suggesting the change of oxidation state of titanium atoms. All the titanium atoms on the surface had an oxidation state of +4, if there was formation of new bonds between titanium and carbon, then, a shift in the Ti $2p_{3/2}$ and Ti $2p_{½}$ to lower binding energies was to be expected. This shift in binding energies can be attributed to the presence of titanium with an oxidation state of +3 which is said to be due to the formation of new bonds in the nanocomposite[21].

Oxygen was present with the highest atomic percentage of 50.8 %, the oxygen can be attributed to both TiO_2 and the nanodiamonds. The O 1s atoms with the highest atomic composition of 42.9 % at peak position 529.5 eV can be attributed to a metal oxide which in this case is titanium dioxide[21]. The remaining two O 1s peaks were organic C-O (4.3 %) and organic C=O (2.0 %) with binding energies of 531.0 eV and 532.3 eV. These two peaks provide evidence that the nanodiamonds had oxygenated surface groups on the graphitic shell. Cl $2p_{3/2}$ (1.4 %) and Cl $2p_{1/2}$ (1.3 %) were present with binding energies of 197.2 eV and 199.2 eV respectively. The peak at 197.2 eV can be attributed to Cl^- ions physically adsorbed on the surface of the composite whereas the peak at 199.2 eV can be attributed to Cl^- ions incorporated into the lattice of TiO_2[22,23]. Incorporating Cl in the TiO_2 matrix could help in the creation of a new impurity level in TiO_2 bandgap thereby increasing photocatalytic efficiency[22]. Chlorine and nitrogen were co-doped on TiO_2 and this increased photocatalytic degradation of rhodamine B and phenol[22]. Chlorine doping was reported to increase photocatalytic efficiency of $ZnWO_4$ on the degradation of methylene blue by Huang and Zhu[23].

Table 4.6: Elemental identification after peak separation

Element	Peak Binding Energy (eV)	Atomic Percentage (%)
O 1s (metal oxide)	**529.5**	**42.9**
O 1s (organic C-O)	**531.0**	**4.3**
O 1s (organic C=O)	**532.3**	**2.0**
C 1s (C-C)	**284.4**	**20.7**
C 1s (C-O)	**286.1**	**3.3**
C 1s (O-C=O)	**288.4**	**2.6**
Ti $2p_{3/2}$ (TiO_2)	**458.2**	**21.6**
Ti $2p_{1/2}$ (TiO_2)	**464.1**	**1.0**
Cl $2p_{3/2}$	**197.2**	**1.4**
Cl $2p_{1/2}$	**199.2**	**1.3**

4.4 References

1. Bai X, Xie B, Pan N, Wang X, Wang H. Novel three-dimensional dandelion-like TiO_2 structure with high photocatalytic activity. *J Solid State Chem*. 2008; 181(3): 450-456.
2. Baloyi J, Seadira T, Raphulu M, Ochieng A. Preparation, Characterization and Growth Mechanism of Dandelion-like TiO_2 Nanostructures and their Application in Photocatalysis towards Reduction of Cr(VI). *Mater Today Proc*. 2015; 2(7): 3973-3987.
3. Baloyi J, Seadira T, Raphulu M, Ochieng A. Synthesis and Characterization of Dandelion-like TiO_2 Structure as Photocatalyst for Industrial Wastewater Treatment Containing Toxic Metal Hg (II). *PsrcentreOrg*. 2014. http://psrcentre.org/images/extraimages/414028.pdf.
4. Bai Y, Liu Z, Zhang N, Sun K. One-pot synthesis of 3-D dandelion-like architectures constructed by rutile TiO_2 nanorods grown along [001] axis for high-rate lithium ion

batteries. *RSC Adv*. 2015; 5(27): 21285-21289.

5. Yi J, Liu Y, Wang Y, Li X, Hu S, Li W. Synthesis of dandelion-like TiO_2 microspheres as anode materials for lithium ion batteries with enhanced rate capacity and cyclic performances. 2012; 19(11): 1058-1062.
6. Zhou J, Zhao G, Han G, Song B. Solvothermal growth of three-dimensional TiO_2 nanostructures and their optical and photocatalytic properties. *Ceram Int*. 2013; 39(7): 8347-8354.
7. Baloyi J, Seadira T, Raphulu M, Ochieng A. Preparation, Characterization and Growth Mechanism of Dandelion-like TiO_2 Nanostructures and their Application in Photocatalysis towards Reduction of Cr(VI). *Mater Today Proc*. 2015; 2(7): 3973-3987.
8. Reddy KM, Manorama S V., Reddy AR. Bandgap studies on anatase titanium dioxide nanoparticles. *Mater Chem Phys*. 2003; 78(1): 239-245.
9. Sampaio MJ, Marques RRN, Tavares PB, Faria JL, Silva AMT, Silva CG. Tailoring the properties of immobilized titanium dioxide/carbon nanotube composites for photocatalytic water treatment. *J Environ Chem Eng*. 2013; 1(4): 945-953.
10. Zou Q, Li YG, Zou LH, Wang MZ. Characterization of structures and surface states of the nanodiamond synthesized by detonation. *Mater Charact*. 2009; 60(11): 1257-1262.
11. Pastrana-Martínez LM, Morales-Torres S, Carabineiro SAC. Nanodiamond-TiO_2 composites for heterogeneous photocatalysis. *Chempluschem*. 2013; 78(8): 801-807.
12. Sampaio MJ, Pastrana-Martinez LM, Silva AMT. Nanodiamond TiO_2 composites for photocatalytic degradation of microcystin-LA in aqueous solutions under simulated solar light. *RSC Adv*. 2015; 5(72): 58363-58370.
13. Ferrari AC, Robertson J. Raman spectroscopy of amorphous, nanostructured, diamond-like carbon, and nanodiamond. *Philos Trans R Soc A Math Phys Eng Sci*. 2004; 362(1824): 2477-2512.
14. Pichot V, Comet M, Fousson E. An efficient purification method for detonation nanodiamonds. *Diam Relat Mater*. 2008; 17(1): 13-22.
15. Kim KD, Dey NK, Seo HO, Kim YD, Lim DC, Lee M. Photocatalytic decomposition of toluene by nanodiamond-supported TiO_2 prepared using atomic layer deposition. *Appl Catal A Gen*. 2011; 408(1-2): 148-155.
16. Ekoi EJ, Gowen A, Dorrepaal R, Dowling DP. Characterisation of titanium oxide layers using Raman spectroscopy and optical profilometry: Influence of oxide properties. *Results Phys*. 2019; 12: 1574-1585.
17. Behera D, Bag B, Sakthivel R. Synthesis, characterization and photoluminescence study

of modified titania. *Indian J Pure Appl Phys*. 2011; 49(11): 754-758.

18. Khaki MRD, Shafeeyan MS, Raman AAA, Daud WMAW. Application of doped photocatalysts for organic pollutant degradation - A review. *J Environ Manage*. 2017; 198: 78-94.
19. Li Y, Hwang DS, Lee NH, Kim SJ. Synthesis and characterization of carbon-doped titania as an artificial solar light sensitive photocatalyst. *Chem Phys Lett.* 2005; 404(1-3): 25-29.
20. Hashimoto K, Irie H, Fujishima A. TiO_2 Photocatalysis: A Historical Overview and Future Prospects. *Jpn J Appl Phys*. 2005; 44(12): 8269-8285.
21. Lee S, Yun CY, Hahn MS, Lee J, Yi J. Synthesis and characterization of carbon-doped titania as a visible-light-sensitive photocatalyst. *Korean J Chem Eng*. 2008; 25(4): 892-896.
22. Cheng X, Yu X, Xing Z, Yang L. Enhanced visible light photocatalytic activity of mesoporous anatase TiO_2 codoped with nitrogen and chlorine. *Int J Photoenergy*. 2012. doi:10.1155/2012/593245
23. Huang G, Zhu Y. Synthesis and photoactivity enhancement of $ZnWO_4$ photocatalysts doped with chlorine. *CrystEngComm*. 2012; 14(23): 8076-8082.
24. Petit T. and Puskar L. FTIR spectroscopy of nanodiamonds: Methods and interpretation. *Diamond and Related Materials*. 2018; 89. 10.1016/j.diamond.2018.08.005.
25. Petrov I., Shenderova O., Grichko V., Tyler T., Cunningham G., McGuire G., Detonation nanodiamonds simultaneously purified and modified by gas treatment. *Diamond and related materials*. 2007; 16(12): 2098-2103
26. Shenderova O., Koscheev A., Zaripov N., Petrov I., Skryabin Y., Detkov P., Turner S., Van Tendeloo G. Surface Chemistry and properties of ozone purified detonation nanodiamonds. *Journal of Physical Chemistry.* 2011; 115: 9827-9837

Chapter 5: Photocatalytic activity

5.1 Degradation rate of synthesized composites

The rate of methyl violet degradation was determined by plotting a graph of C/C_0 (rate of dye degradation) versus irradiation time (Figure 5.1), where C_0 is the initial concentration, i.e. 50 ppm and C is the concentration at any given time. A control experiment was done on methyl violet in the presence of solar radiation, without a photocatalyst and the dye concentration did not change. EDS and XPS confirmed the presence of Cl in the composite in the current study. Chlorine and nitrogen were co-doped on TiO_2 in a similar study and this increased photocatalytic degradation of rhodamine B and phenol[1]. Chlorine doping was also reported to increase photocatalytic efficiency of $ZnWO_4$ on the degradation of methylene blue by Huang and Zhu[2]. Incorporation of Cl in the TiO_2 matrix could help in the creation of a new impurity level in TiO_2 bandgap, thereby increasing photocatalytic efficiency[1].

The choice of degradation parameters for the composites was based on the photodegradation studies that were done on RANR TiO_2 in this current project (Fig. 5.3 and 5.5) as well as parameters reported in literature[4,12,13,14]. The reactions were done using 10 mg of composite catalysts and 50 ml of 50 ppm methyl violet for 140 minutes using a solar simulator. Methyl violet degradation was done for 140 minutes to allow for the photocatalytic reaction to complete as shown by the levelling of the degradation rate (Fig. 5.1).

Nanodiamonds have been reported in literature to be photocatalytic active if the surface is modified, e.g. by acidification[15,16], hydrogenation[3] or oxidation[3]. In this study, detonated nanodiamonds were used without surface modification since they already had functional groups present as evidenced by FTIR results. The nanodiamonds were only active in the first 20 minutes of the reaction as shown in Figure 5.1. They showed to be good adsorbents, because

they adsorbed a large amount of dye in darkness when the solution was being homogenized, before illumination, compared to other catalysts. The high adsorbance of the nanodiamonds in the dark can be attributed to their high BET surface area of 244 m^2/g which creates more adsorption sites. The low efficiency (29 %) of nanodiamonds on their own could also be attributed to their large band gap energies, which are approximately 5 eV[4]. H_2 treated nanodiamonds were reported to be highly photocatalytic active towards H_2 production by reduction of water, this was attributed to the action of H-terminated sites as electron reservoirs[3].

Table 5.1: Degradation efficiencies using 50 ml, 50 ppm methyl violet and 10 mg of synthesized photocatalysts at 140 minutes

Material	Degradation efficiency %
RANR TiO_2 (dandelions)	**97**
TND 0.1%	**89**
TND 0.5%	**87**
TND 1%	**86**
TND 0.1%, 200 °C	**90**
TND 0.5%, 200 °C	**88**
TND 1%, 200 °C	**87**

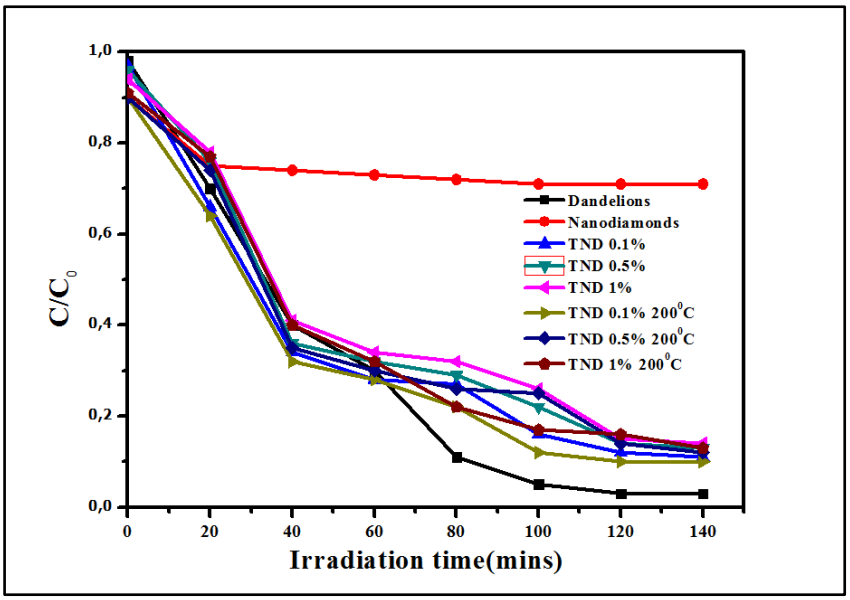

Figure 5.1: Graph showing rate of dye degradation of methyl violet against irradiation time for the synthesized composites.

RANR TiO_2 (dandelions) were the most effective in photocatalytic degradation of methyl violet with a degradation efficiency of 97 % after irradiation time of 140 minutes (Figure 5.1). This can be attributed to the high surface areas (S_{BET} = 68 m^2/g) of the dandelion-like structures which gives the TiO_2 strong light absorption capacity. The dandelion-like morphology favours multi-reflections on the nano rods which improves production of charge carriers[5]. The high surface areas of RANR TiO_2 increase photocatalytic activity because of the presence of more surface-active sites for adsorption of the dye (reactant), easy transportation of reactant and product molecules through the pores[6].

Modification of the dandelions with 0.1 wt.% nanodiamonds increased the rate of dye degradation in the first hour as shown in Figure 5.1, due to the increase in surface area from 68 m^2/g to 83 m^2/g. The increase in weight percentage from 0.1% to 1% led to a decrease in degradation rate because from the TEM images obtained, some of the nanodiamonds were not attached to the rods as the weight percentage was increased. The nanodiamonds could have

decreased the degradation rate since they were shown not to be efficient on their own. All the other composites did generally well with respect to dandelions in the first 60 minutes (Figure 5.1), however, the rate of degradation decreased after 60 minutes which could be attributed to the reduction in photocatalytic active sites due to accumulation of reactants and reaction intermediates on the catalyst surfaces.

The functional groups on the surface of the nanodiamonds that were determined by XPS and FTIR, e.g. -OH and other oxygen containing groups create a surface dipole layer that can affect the composite interface electron affinity. The presence of hydrogen bonds on H-terminated nanodiamond surfaces could shift the conduction band above the vacuum energy level. The electrons can then be transferred directly to the surrounding media via surface states[7]. A good dispersion of the nanodiamonds and RANR TiO_2 (0.1 % loading) can help create strong electronic interphase interactions, i.e. transfer of electrons from the nano diamonds CB to the RANR TiO_2 CB, and also, the transfer of RANR TiO_2 holes from the VB to the nanodiamonds VB. This helps to separate the photogenerated electrons and positive holes thereby increasing photocatalytic efficiency[4]. Calcination helped to increase photocatalytic efficiency thereby rate of degradation was also increased in all cases this was due to the increase in crystallinity of the composites as shown by Raman analysis which helps to reduce electron/hole recombination.

5.2 Effect of varying amount of photocatalyst

RANR TiO_2 was used to study the effect of varying the amount of photocatalyst, since it showed the highest degradation efficiency, compared to the other composites. The photocatalyst mass was varied between 5 mg and 20 mg, using 10 ppm of methyl violet as shown in the Uv-vis data in Figure 5.2. Photocatalytic dye degradation efficiency was found to be proportional to the amount of photocatalyst used (Figure 5.3). An increase in amount of

catalyst also increased degradation efficiency. The photocatalyst with mass of 40 mg showed the highest efficiency (99 %) at 60 minutes (Figure 5.3). The high amount of photocatalyst led to an increase in the number of active sites on the photocatalyst surface. The increase in the active sites resulted in an increase in the hydroxide and superoxide radicals produced.

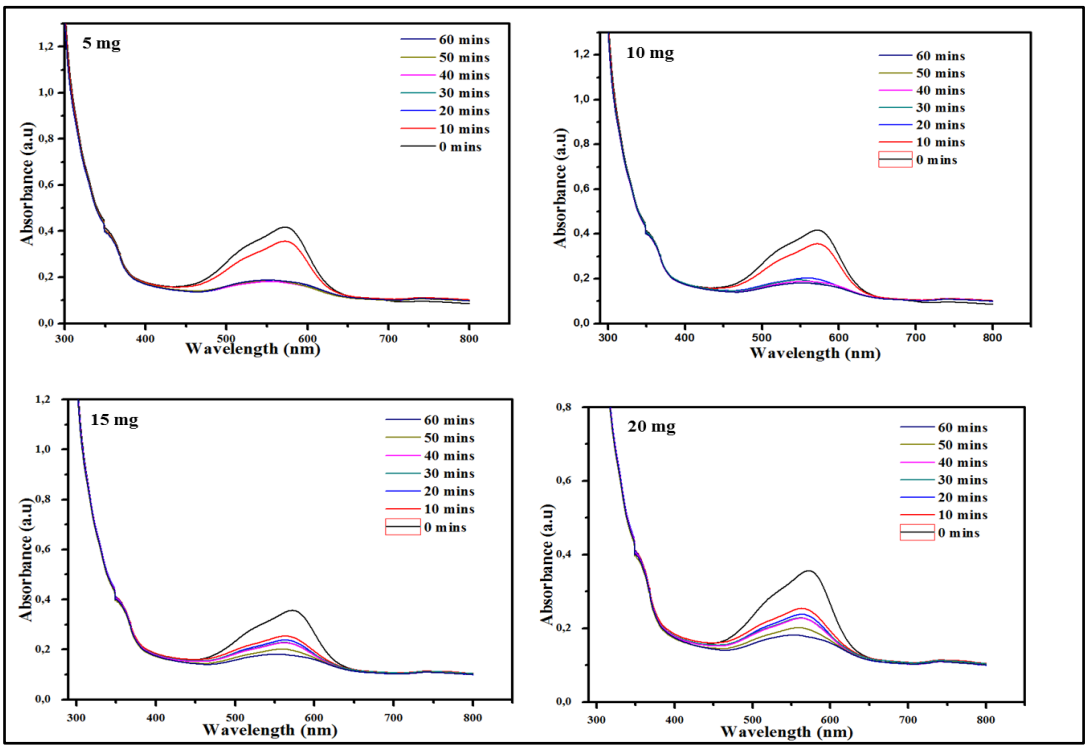

Figure 5.2: UV-Vis graphs for effect of amount of catalyst on degradation efficiency study.

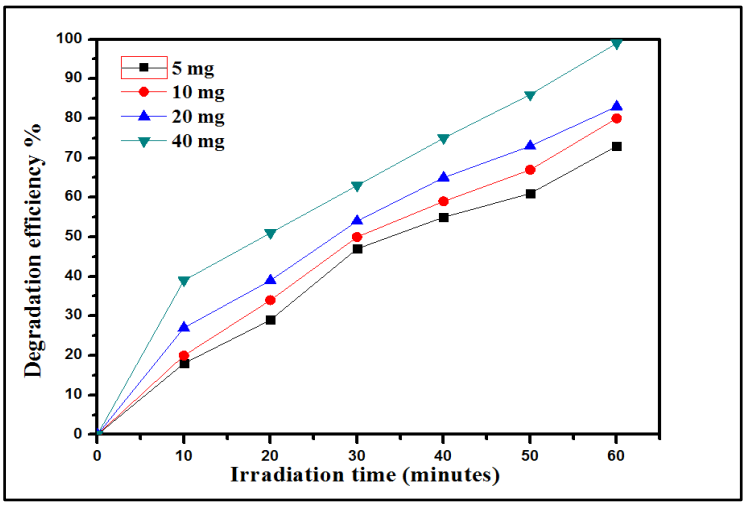

Figure 5.3: Graph showing the effect of mass of RANR TiO_2 on degradation efficiency in 50 ml of 10 ppm methyl violet.

5.3 Effect of initial dye concentration

The concentration of methyl violet was varied between 5 ppm and 40 ppm in order to determine the effect of increasing dye concentration on the degradation efficiency as shown in Figure 5.4 and 5.5. The 5 ppm dye solution had the highest degradation efficiency of 90 % followed by 10 ppm, 20 ppm and lastly 40 ppm with 65% efficiency at 60 minutes (Figure 5.5). The degradation efficiency was found to be inversely proportional to the concentration of methyl violet. This is because as the concentration of the dye is increased, the competitive adsorption of $-OH^-$ on the active sites of the catalyst decreases as the equilibrium adsorption of dye on the active sites increases. This leads to a reduction in the formation rate of the OH• radical hence a decrease in degradation efficiency[9]. A similar trend was also reported by Baloyi et al. of the decrease in reduction rate of Cr (VI) with increase in initial dye concentration[8].

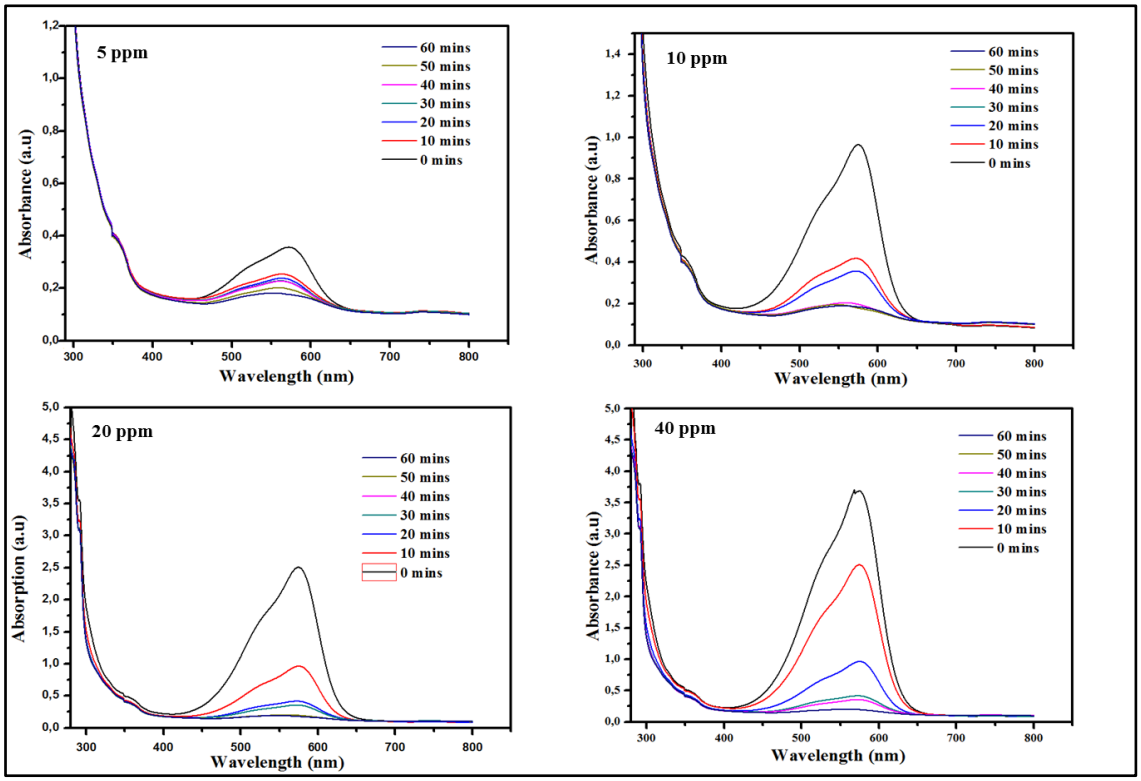

Figure 5.4: UV-Vis graphs for effect of increasing dye concentration on degradation efficiency study.

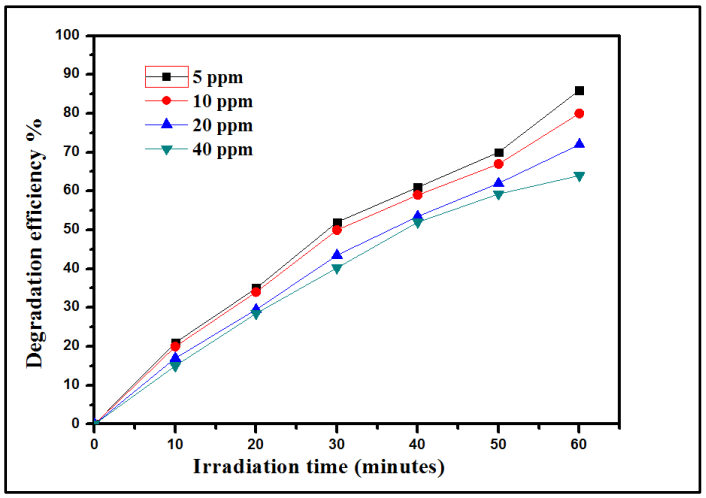

Figure 5.5: Degradation efficiency graph for varied dye concentrations using 10 mg RANR TiO_2.

5.4 Recyclability studies

The RANR TiO_2 photocatalyst (10 mg in 50 ml, 10 ppm methyl violet) was re-used 3 times after the initial experiment. All the reactions were run for 60 minutes as shown in the graph in Figure 5.6 and 5.7. The recyclability studies showed that the recovery of the catalyst after each cycle was not 100% effective hence the re-use was also not effective. The degradation efficiency of the photocatalyst decreased from 80 % to 60 % after the third cycle (Figure 5.7). The degradation rate also decreased with increase in number of cycles suggesting that some of the photocatalyst active sites were blocked after the end of each cycle hence lower degradation efficiency.

Recovering the catalyst after each cycle was a challenge since some of the photocatalyst was lost during washing with distilled water before re-use in the next cycle. Some of the catalyst was also lost when aliquots were drawn during the course of each reaction. The decrease in efficiency of the photocatalyst can also be attributed to loss of catalyst at the end of each cycle. A similar trend in recyclability was also observed by Teixeira et.al., a decrease in degradation

efficiency after 3 cycles using TiO_2 and ZnO nanoparticles was reported[10]. The photocatalytic activity of Au-TiO_2 in the degradation of methyl blue over 10 cycles, as reported in a similar study[11].The excellent activity was attributed to the effective cleaning of active sites of the catalyst by photodegradation before the next cycle[11].

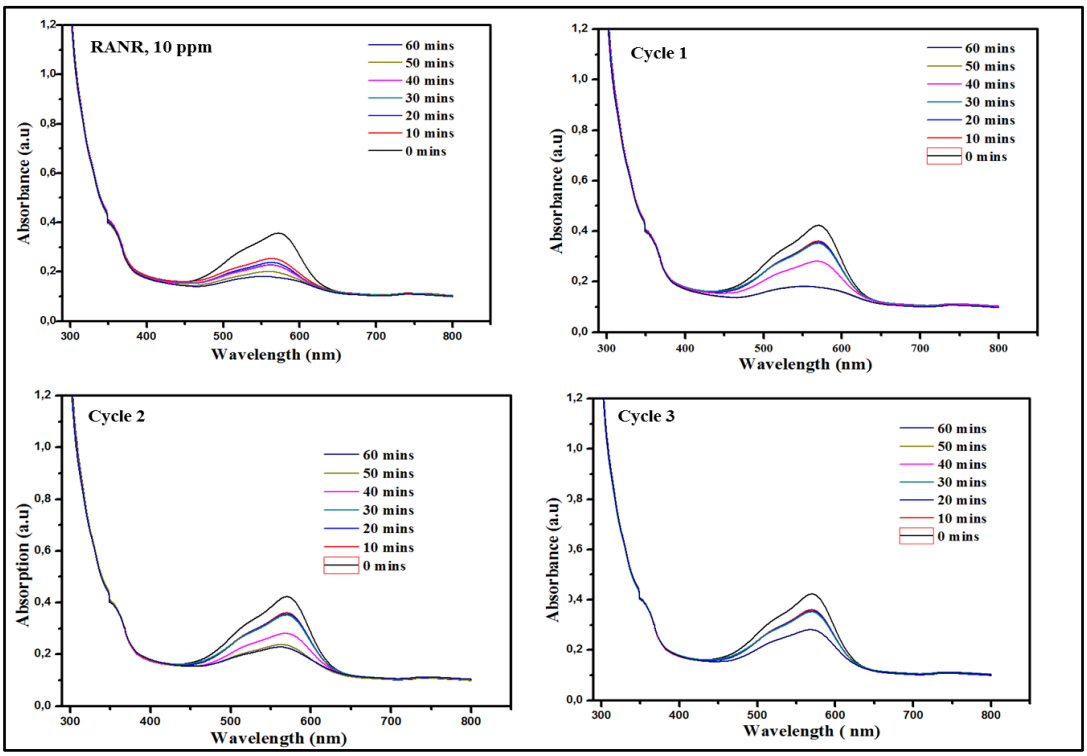

Figure 5.6: Graph showing UV-Vis data for recyclability studies for the photocatalyst.

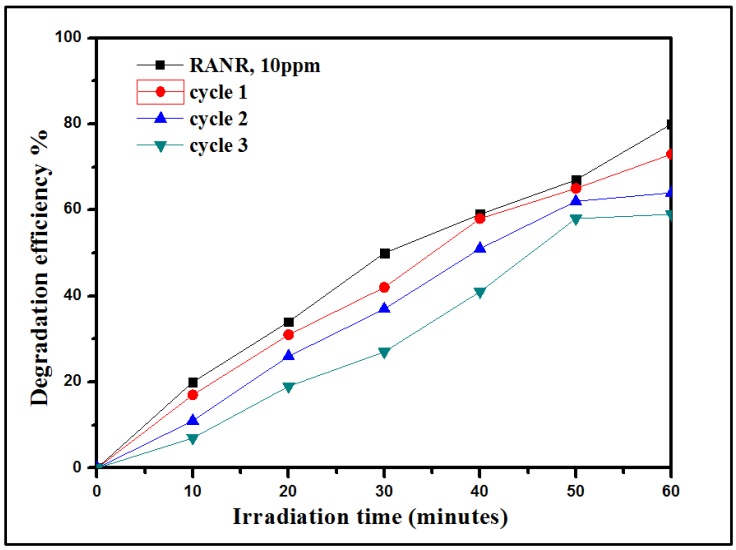

Figure 5.7: Degradation efficiency graph for recycled photocatalyst using 10 mg catalyst and 50 ml of 10 ppm methyl violet.

5.5 References

1. Cheng X, Yu X, Xing Z, Yang L. Enhanced visible light photocatalytic activity of mesoporous anatase TiO_2 codoped with nitrogen and chlorine. *Int J Photoenergy*. 2012; 2012.

2. Huang G, Zhu Y. Synthesis and photoactivity enhancement of $ZnWO_4$ photocatalysts doped with chlorine. *CrystEngComm*. 2012; 14(23): 8076-8082.

3. Jang DM, Myung Y, Im HS. Nanodiamonds as photocatalysts for reduction of water and graphene oxide. *Chem Commun*. 2012; 48(5): 696-698.

4. Sampaio MJ, Pastrana-Martinez LM, Silva AMT. Nanodiamond TiO_2 composites for photocatalytic degradation of microcystin-LA in aqueous solutions under simulated solar light. *RSC Adv*. 2015; 5(72): 58363-58370.

5. Baloyi J, Seadira T, Raphulu M, Ochieng A. Preparation, Characterization and Growth Mechanism of Dandelion-like TiO_2 Nanostructures and their Application in Photocatalysis towards Reduction of Cr(VI). *Mater Today Proc*. 2015; 2(7): 3973-3987.

6. Bai X, Xie B, Pan N, Wang X, Wang H. Novel three-dimensional dandelion-like TiO_2 structure with high photocatalytic activity. *J Solid State Chem*. 2008; 181(3): 450-456.

7. Kim KD, Dey NK, Seo HO, Kim YD, Lim DC, Lee M. Photocatalytic decomposition of toluene by nanodiamond-supported TiO_2 prepared using atomic layer deposition. *Appl Catal A Gen*. 2011; 408(1-2): 148-155.

8. Baloyi J, Seadira T, Raphulu M, Ochieng A. Preparation, Characterization and Growth Mechanism of Dandelion-like TiO_2 Nanostructures and their Application in Photocatalysis towards Reduction of Cr(VI). *Mater Today Proc*. 2015; 2(7): 3973-3987.

9. Akyol A, Yatmaz HC, Bayramoglu M. Photocatalytic decolorization of Remazol Red RR in aqueous ZnO suspensions. *Appl Catal B Environ*. 2004; 54(1): 19-24.

10. Teixeira S, Martins PM, Lanceros-Méndez S, Kühn K, Cuniberti G. Reusability of photocatalytic TiO_2 and ZnO nanoparticles immobilized in poly(vinylidene difluoride)-co-trifluoroethylene. *Appl Surf Sci*. 2016; 384: 497-504.

11. Padikkaparambil S, Narayanan B, Yaakob Z, Viswanathan S, Tasirin SM. Au/TiO_2

reusable photocatalysts for dye degradation. *Int J Photoenergy*. 2013. doi:10.1155/2013/752605

12. Dziike F, Franklyn P, Durbach S, Maubane M, Hlekelele L, Synthesis of Radially Aligned Nano-rutile Modified with Au and Ni for the Photodegradation of Methyl Orange. *Materials Research Bulletin*. 2018; 104. 10.1016/j.materresbull.2018.04.016.

13. Pastrana-Martínez LM, Morales-Torres S, Carabineiro SAC. Nanodiamond-TiO_2 composites for heterogeneous photocatalysis. *Chempluschem*. 2013; 78(8): 801-807.

14. Chang BYS, Mehmood MS, Pandikumar A, Huang NM, Lim HN, Marlinda R, Yusoff N, Chiu WS, Hydrothermally prepared graphene-titania nanocomposite for the solar photocatalytic degradation of methylene blue, *Desalination and Water Treatment*, 2016; 57(1), 238-245

15. Pichot V, Comet M, Fousson E. An efficient purification method for detonation nanodiamonds. *Diam Relat Mater*. 2008; 17(1): 13-22.

16. Bogatyreva GP, Marinich MA, Ishchenko E V., Gvyazdovskaya VL, Bazalii GA, Oleinik NA. Application of modified nanodiamonds as catalysts of heterogeneous and electrochemical catalyses. *Phys Solid State*. 2004; 46(4): 738-741.

Chapter 6: Results summary

6.1 Material synthesis

Rutile TiO_2 nanorods with dandelion-like structures were successfully synthesized at an optimum temperature of 180 °C for 16 hours using a hydrothermal method. The dandelions had diameters ranging from 300 nm to 800 nm and an average diameter of 560 nm. The synthesis time was kept at 16 hours for all other materials that were synthesized because the samples that were synthesized below 16 hours had half shaped dandelion structures. This was also true for materials that were synthesized below 180 °C, which leads to the conclusion that nanorods growth and dandelion formation is dependent on both temperature and reaction time.

The BET results show that the synthesized dandelions had higher surface areas (68 m^2/g) as compared to the commercially available p25 (45 m^2/g). This is due to the morphology of the RANR TiO_2 which is also three dimensional. SEM and TEM were used to confirm the morphology of the RANR TiO_2 which was found to be dandelion-like. TEM results obtained from the aliquots collected every 4 hours as the reaction proceeded showed that nucleation and growth were responsible for the formation of the dandelions. The rods grow and self-align radially forming half-dandelions which then fully grow to become dense dandelion-like structures as shown in the figure below. XRD confirmed the presence of rutile in the synthesized materials. The TiO_2 samples that were synthesized at temperatures below 180 $^{\circ}C$ were all pure rutile, but as synthesis temperatures were increased, a mixture of rutile and anatase was formed with mainly rutile. This contradicts claims which were made in literature, but, from the XRD results that were obtained, it is possible to produce anatase at high

temperatures, and that the polymorphs that are formed not only depend on temperature, but also depend on the synthesis method used and the reaction conditions.

The characterization techniques used showed positive results which confirmed the presence of nanodiamonds. XRD confirmed the presence of diamond grains since all the peaks that were present were matched to diamond. BET was also useful in determining the surface area of the nanodiamonds which was found to be 244 m^2/g. The detonation nanodiamonds had impurities, and nitrogen was one of the main impurities. The Raman spectra obtained supports this because several overlapping fluorescence peaks were present which were due to the present of nitrogen vacant sites in the nanodiamonds core. XPS confirmed the presence of 0.4% Nitrogen (N Is) on the surface of the nanodiamonds. The presence of oxygenated surface groups on the nanodiamonds surface was also confirmed by XPS and FTIR.

The TiO_2-nanodiamond composites were all synthesized in situ using the hydrothermal method with nanodiamonds ranging from 0.1% to 1% loading. TEM results show that calcination of the composite above 200 °C leads to a loss in shape of the nanorods and a formation of a spherical morphology with low surface areas which was not desired. BET surface area analysis shows an increased surface area after modification of the RANR TiO_2 using the nanodiamonds. Raman spectra confirmed the presence of graphitic carbon and rutile in all the composite samples. XPS was used to determine the elements present in one of the composite samples with 1% loading and to confirm if any bonds were formed between titanium and carbon. The XPS results showed the presence of carbon, titanium, oxygen and chlorine on the surface of the composite but did not show any evidence that Ti-C bonds were present in the material. All the Ti 2p peaks in the nanocomposite were for titanium in the +4 oxidation state and they had the same binding energies as pure rutile. A change in oxidation state or a shift in the binding

energies would have meant the presence of Ti-C bonds. The carbon (C 1s) peaks that were present on the composite surface were all from the nanodiamonds.

6.2 Photocatalysis

In this study, detonation nanodiamonds were used without surface modification since they already had functional groups as evidenced by FTIR and XPS. The nanodiamonds were not photocatalytic active, but they showed to be a good adsorbent material because they adsorbed a large amount of dye in darkness when the solution was being homogenized before illumination as compared to other catalysts. The high adsorbance of the nanodiamonds in the dark can be attributed to their high BET surface areas of 244 m^2/g. The low efficiency of nanodiamonds on their own could be attributed to their large band gap energies which are approximately 5 eV.

Dandelions were the most effective in dye degradation due to the nanorod structure which increases light harvesting properties from multiple reflections. All the other composites did generally well with respect to dandelions in the first hour but then the rate of degradation decreased which could be attributed to the reduction in photocatalytic active sites due to blockage by reactants. A good dispersion of the nanodiamonds and RANR TiO_2 (0.1% loading) helped to create strong electronic interphase interactions i.e. transfer of electrons from the nano diamonds CB to the RANR TiO_2 CB, and also the transfer of RANR TiO_2 holes from the VB to the nanodiamonds VB. This helps to separate the photogenerated electrons and positive holes thereby increasing photocatalytic efficiency.

Calcination increased photocatalytic efficiency because calcination increases crystallinity of materials which helps to reduce electron/hole recombination. Photocatalytic dye degradation

efficiency was found to be directly proportional to the amount of photocatalyst used whereas degradation efficiency was inversely proportional to the concentration of methyl violet. The photocatalyst recyclability studies showed that the recovery of the catalyst after each cycle was difficult because some of the catalyst was lost during washing with distilled water before re-use. The re-use was not effective as the degradation efficiency decreased from 80% to 60% after 3 cycles.

Chapter 7: Conclusion and future studies

7.1 Concluding statements

- Optimization of RANR TiO_2 synthesis by varying refluxing time and temperature was successful. The optimum reflux temperature was 180 °C for 16 hours using the hydrothermal method.
- In-situ modification of RANR TiO_2 with different amounts of nanodiamonds ranging from 0.1% to 1% was done and the composites were used in photocatalytic degradation of methyl violet.
- Modification of RANR TiO_2 with nanodiamonds helped to increase the rate of photocatalytic methyl violet degradation in the first hour, however, RANR TiO_2 showed the highest photocatalytic efficiency after 140 minutes.

7.2 Future studies/ research

- Further kinetic studies to account for the formation of anatase at temperatures higher than 200 °C.
- A study to come up with a more effective way to wash off all chloride ions from the RANR TiO_2 since washing off several times with warm distilled water did not completely get rid of all the chlorine.
- A study to determine the effect of the chlorine present in the composite on the overall photocatalytic efficiency.
- Studies to improve the interaction between RANR TiO_2 and nanodiamonds by tuning the surface groups on the nanodiamond graphitic shells.

Appendix A

Additional PXRD data for commercially available TiO_2 p25 and other synthesized TiO_2 catalysts at various temperatures.

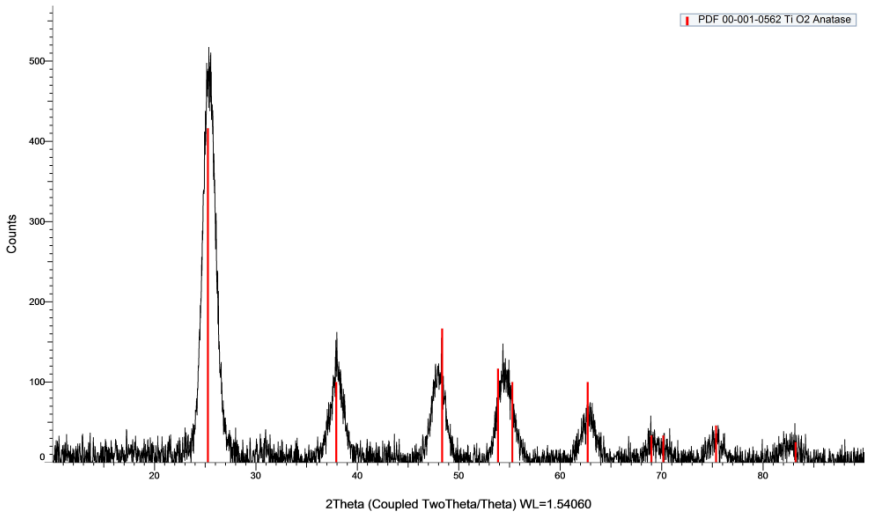

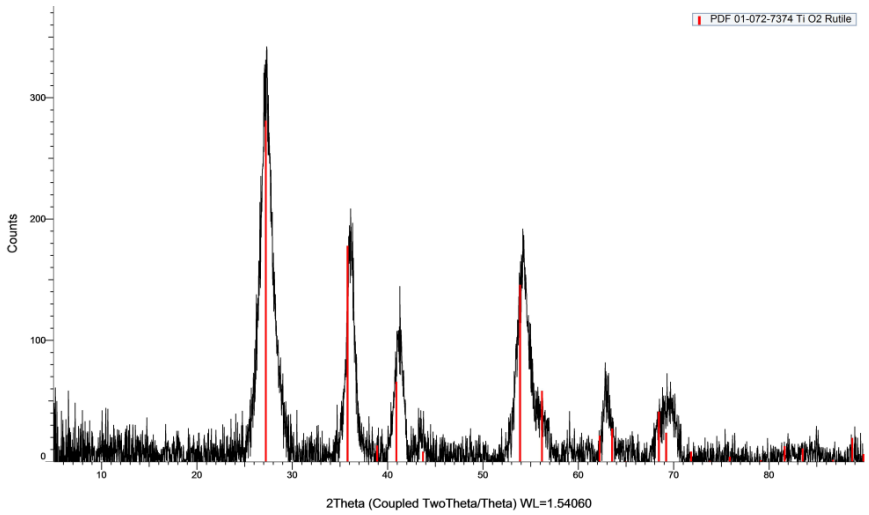

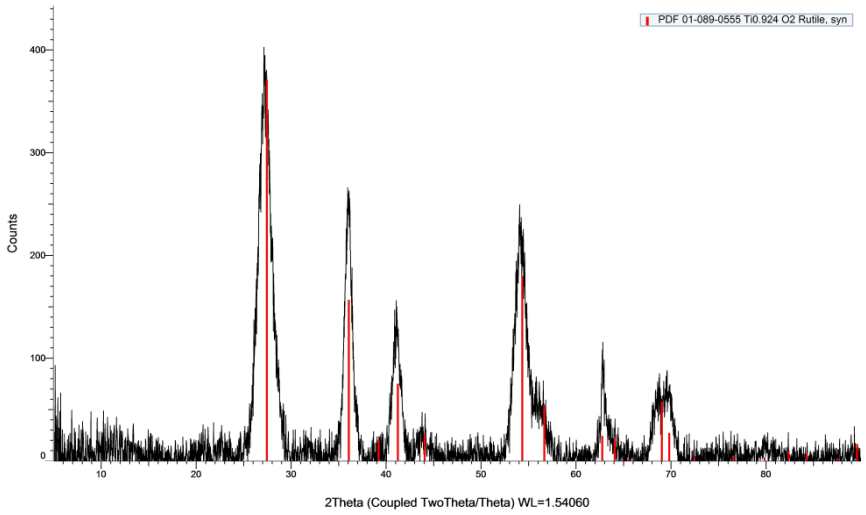

PXRD graphs for p25, TiO_2 catalysts synthesized at 50 °C and 80 °C for 16 hours.

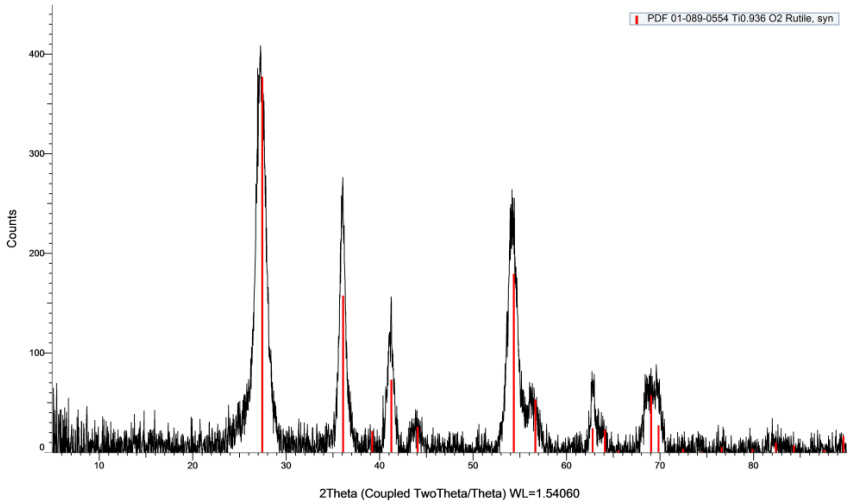

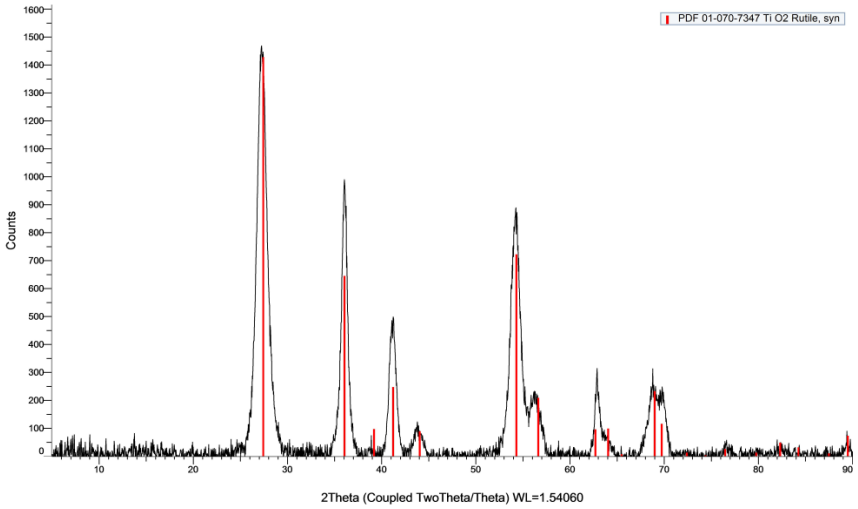

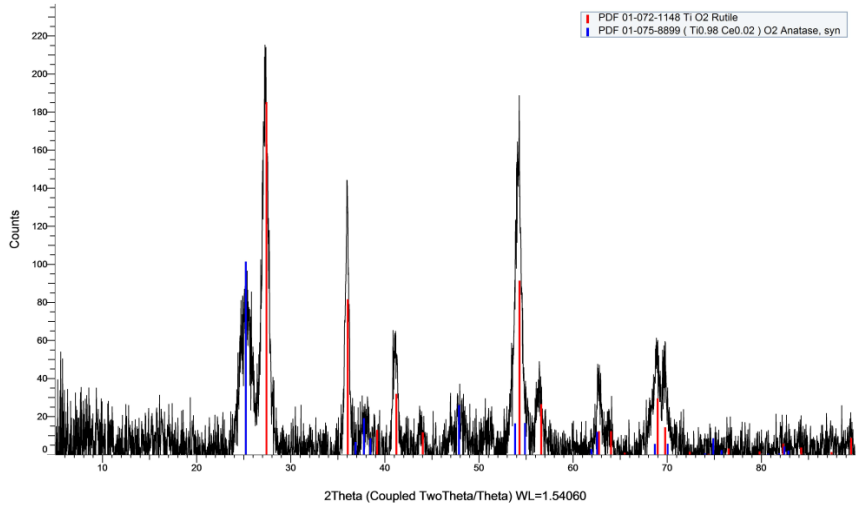

PXRD graphs for TiO_2 catalysts synthesized at 100 °C, 125 °C and 135 °C for 16 hours.

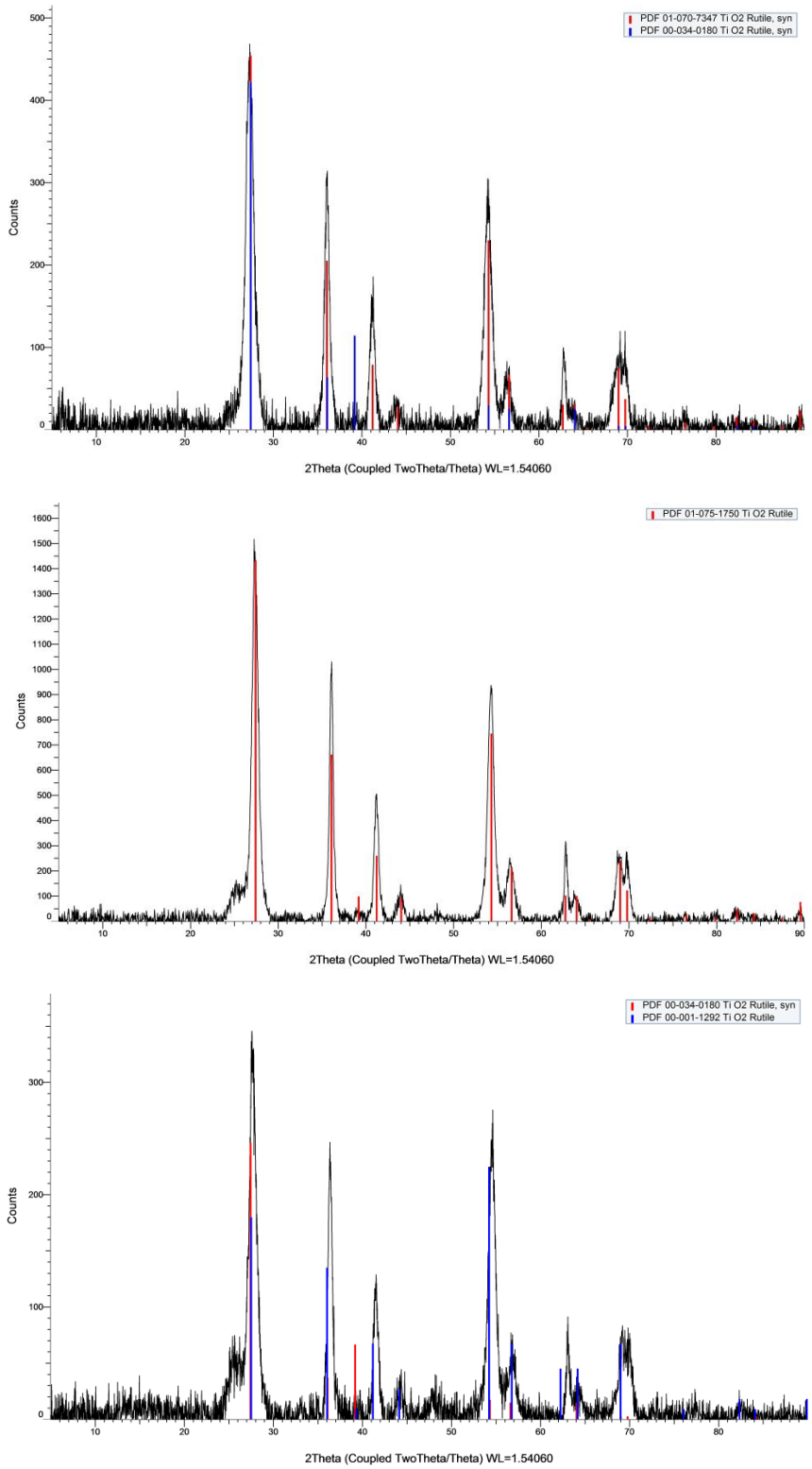

PXRD graphs for TiO_2 catalysts synthesized at 140 °C, 180 °C and 195 °C for 16 hours.

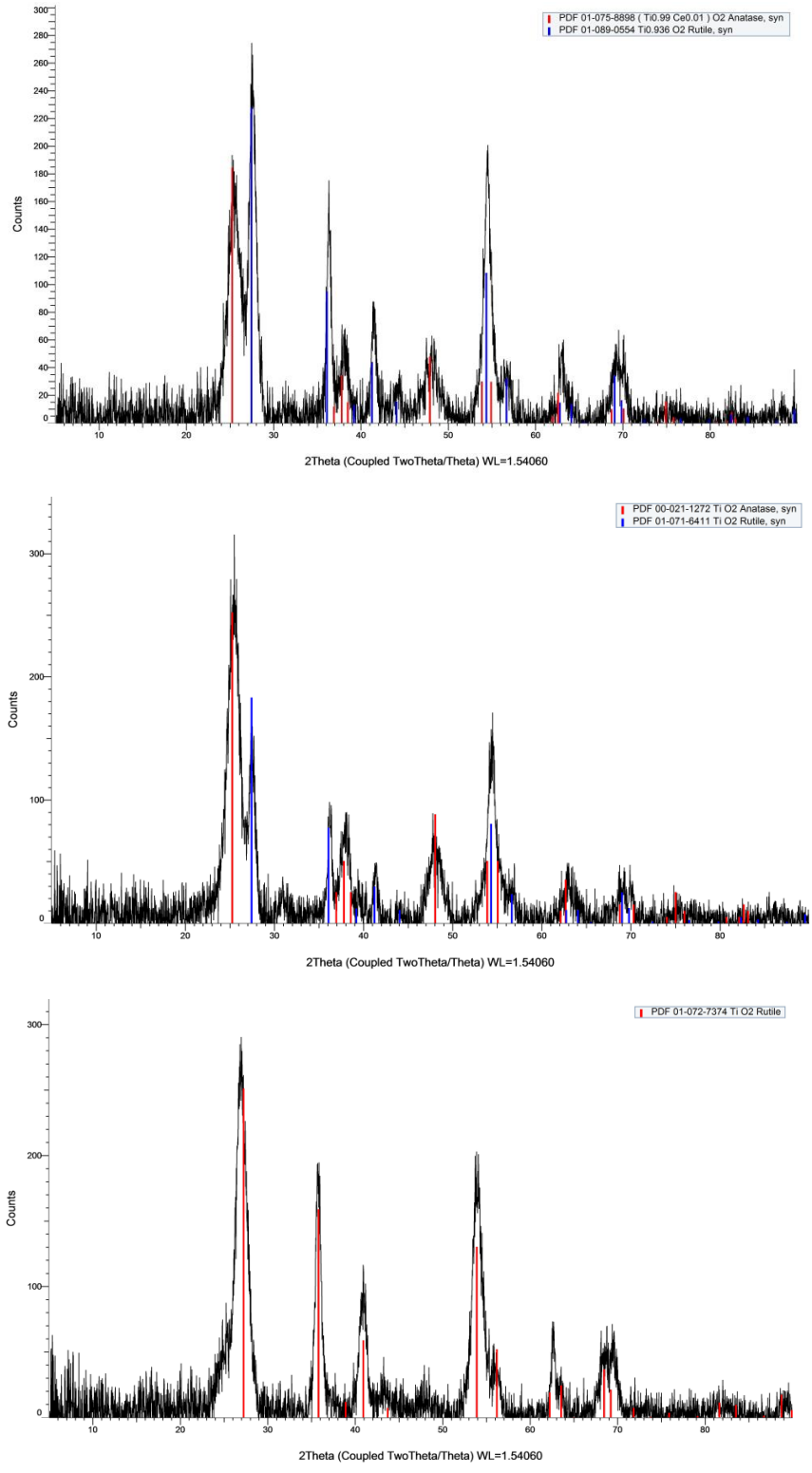

PXRD graphs for TiO_2 catalysts synthesized at 210 °C, 235 °C for 16 hours and 180 °C for 4 hours.

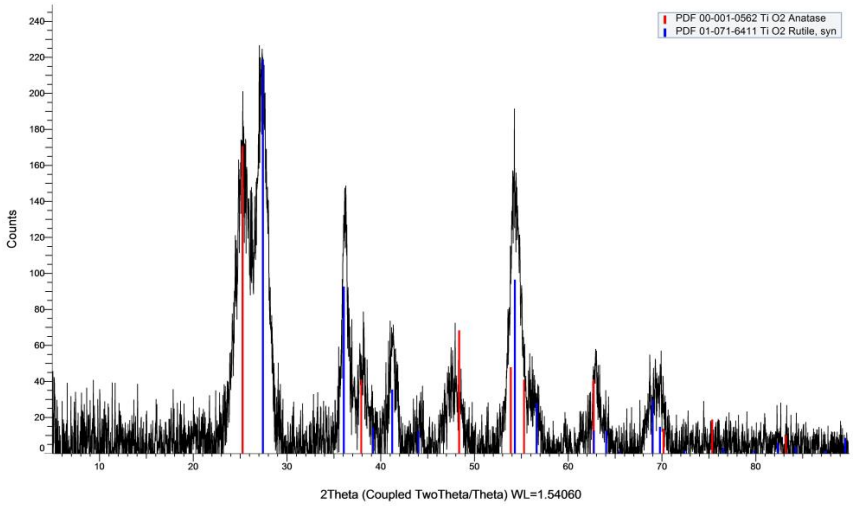

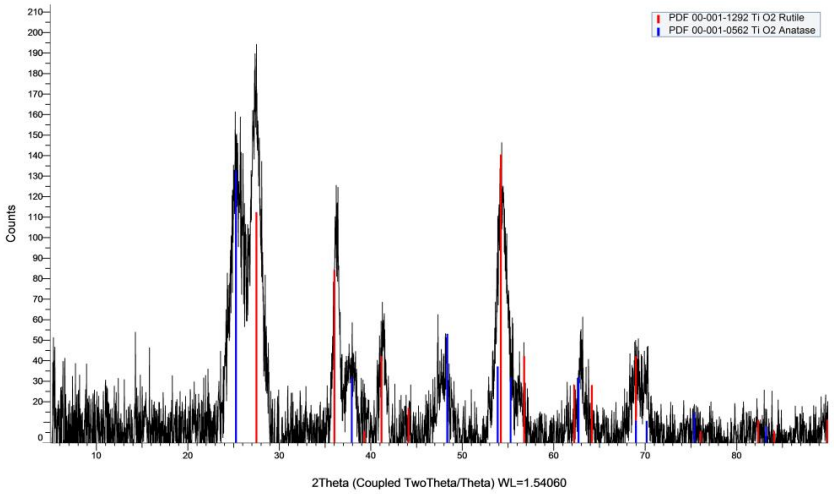

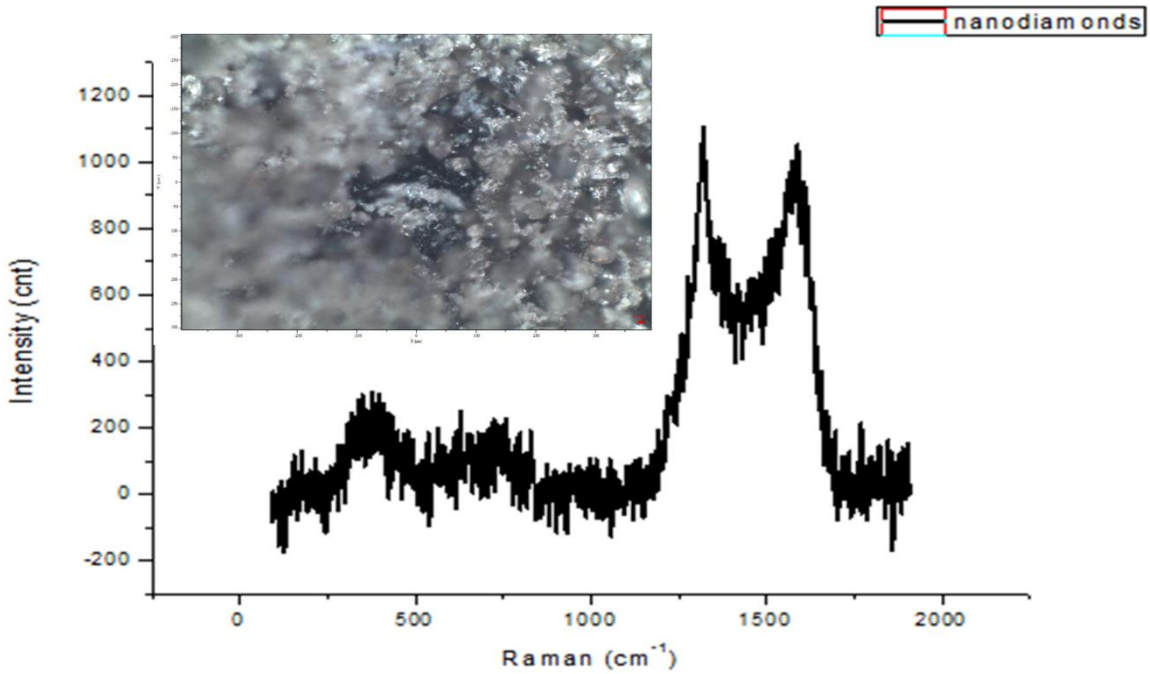

PXRD graphs for TiO_2 catalysts synthesized at 180 °C for 8 and 12 hours. Rama graph and image for nanodiamonds.

Appendix B

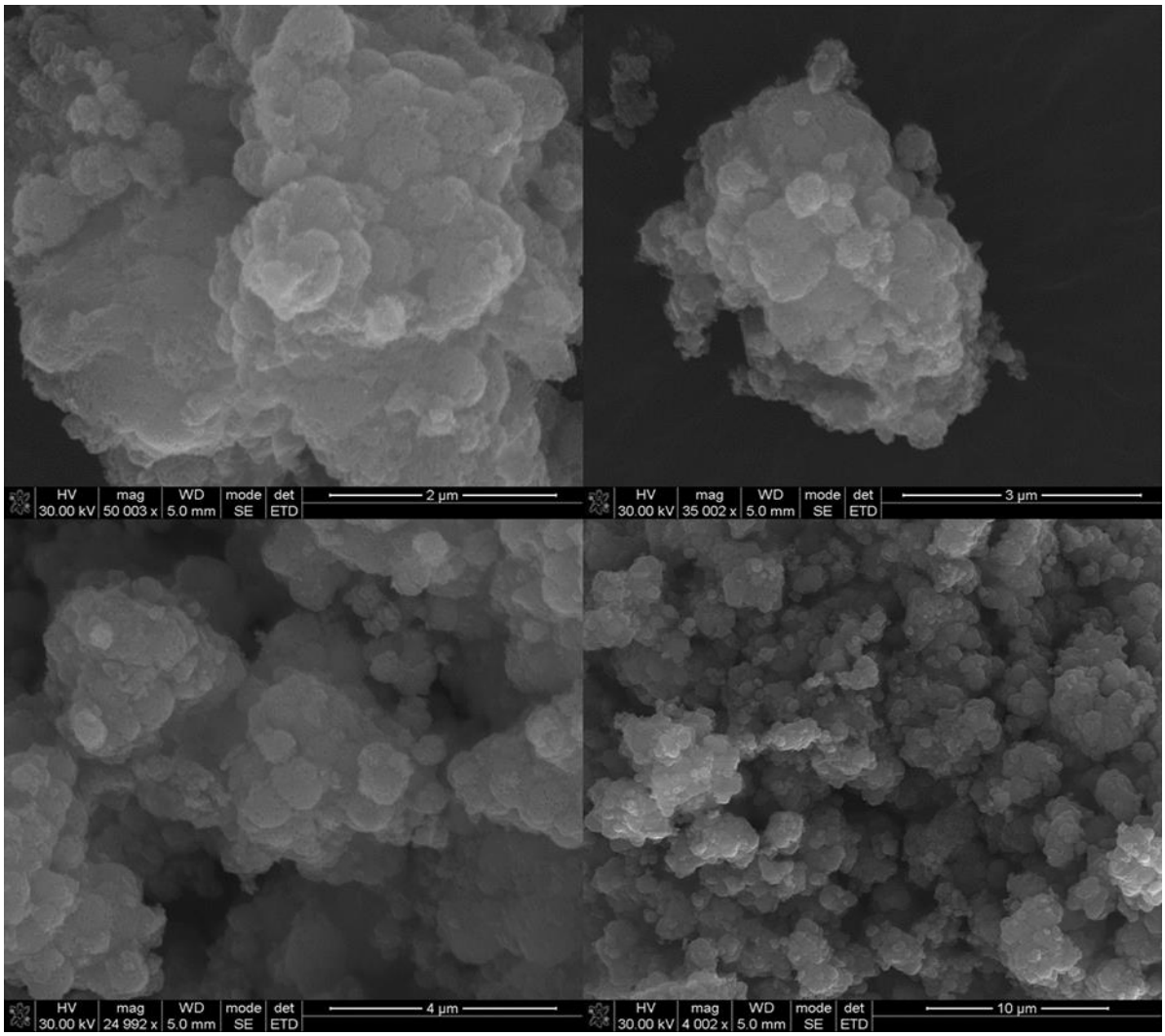

SEM images for synthesized RANR TiO_2 at 180 ℃ for 16 hours

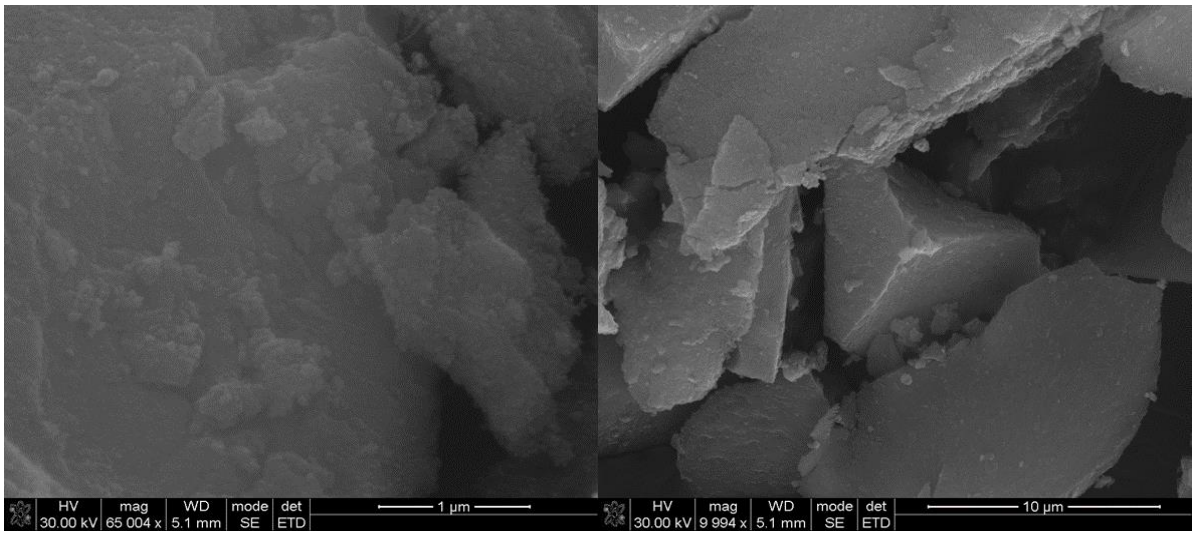

SEM images for synthesized RANR TiO_2 at 210 ℃ for 16 hours

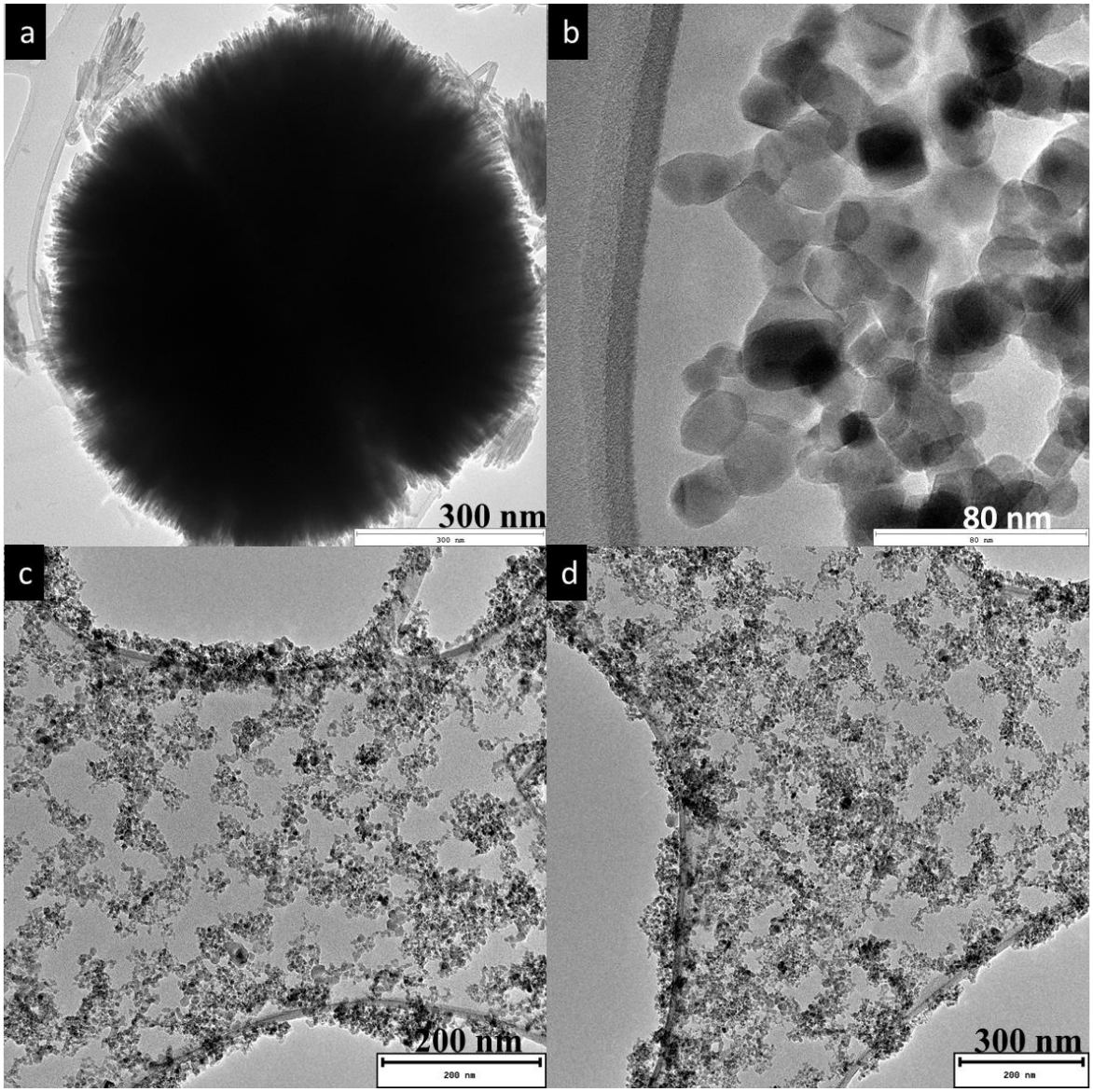

TEM images for synthesized RANR TiO_2(a), P25 (b) and nanodiamonds (c and d)

Appendix C

UV-Vis data for methyl violet photocatalytic degradation studies

Concentration Analysis Report

Report time	2018/11/28 09:45:01 AM
Instrument Settings	
Instrument	Cary 100
Instrument version no.	12.0
Wavelength (nm)	464.00
Ordinate Mode	Abs
SBW (nm)	1.5
Ave Time (sec)	0.10
Beam mode	Double auto select
Beam interchange	Normal
Replicates	2
Standard/Sample averaging	OFF
Weight and volume corrections	OFF
Fit type	Linear
Min R\f1\'b2	0.95000
Concentration units	ppm

Zero Report

Read	Abs		nm	
Zero	(0.0114)	464.00		

Calibration

Collection time		2018/11/28 09:4	5:36 AM

Standard	Concentration ppm	F	Mean	SD	%R	SD	Readings	
1							-0.0005	
	0.0		-0.0005		0.0000	-9.6	-0.0004	
Std 2							0.0343	
	2.0		0.0342		0.0000	0.10	0.0342	
Std 3							0.0963	
	4.0		0.0962		0.0001	0.13	0.0961	
Std 4							0.1130	
	6.0		0.1131		0.0002	0.17	0.1133	
Std 5							0.1346	
	8.0		0.1346		0.0000	0.00	0.1346	
Std 6							0.1924	
	10.0		0.1924		0.0001	0.04	0.1923	

Calibration eqn	Abs	#FIELD!	*Conc +	0.00342
Correlation Coefficient	0.9	7115		
Calibration time	2018/11/28 09:52: 30 AM			

Analysis

Collection time 2018/11/28 09:52:30 AM

Sample	Concentration ppm	F	Mean	SD	%R	SD	Readings
Sample 1							0.0617
		3.2	0.0617	0.0000	0.07		0.0617
Sample 2							0.0469
		2.4	0.0471	0.0002	0.52		0.0473
Sample 3							0.0241
		1.1	0.0243	0.0003	1.03		0.0245
Sample 4							0.0134
		0.5	0.0134	0.0000	0.21		0.0133
Sample 5							0.0081
		0.3	0.0082	0.0001	0.85		0.0082
Sample 6							0.0082
		0.3	0.0082	0.0000	0.61		0.0081
Sample 7							0.1493
		8.0	0.1494	0.0001	0.07		0.1495
Sample 8							0.4166
		22.6 O	0.4167	0.0001	0.02		0.4167

Sample 9					0.4048
	21.9 O	0.4050	0.0002	0.06	0.4051
Sample 10					0.9425
	51.2 O	0.9418	0.0010	0.11	0.9411
Sample 11					0.1410
	7.5	0.1412	0.0003	0.21	0.1414
Sample 12					0.0319
	1.6	0.0320	0.0001	0.41	0.0321
Sample 13					0.0887
	4.6	0.0884	0.0004	0.43	0.0881
Sample 14					0.0345
	1.7	0.0344	0.0001	0.29	0.0344
Sample 15					0.0512
	2.6	0.0516	0.0006	1.14	0.0521
Sample 16					0.0460
	2.3	0.0461	0.0001	0.24	0.0462
Sample 17					0.0150
	0.6	0.0152	0.0003	2.00	0.0154
Sample 18					0.0146
	0.6	0.0148	0.0002	1.65	0.0150

Sample 19			0.0601
	3.1	0.0603 0.0002 0.36	0.0604
Sample 20			0.3106
	16.8 O	0.3106 0.0000 0.01	0.3106
Sample 21			0.5363
	29.1 O	0.5360 0.0003 0.06	0.5358
Sample 22			0.3007
	16.2 O	0.3009 0.0003 0.09	0.3011
Sample 23			0.2090
	11.1	0.2076 0.0020 0.96	0.2062
Sample 24			0.0692
	3.6	0.0695 0.0005 0.66	0.0698
Sample 25			0.1642
	8.8	0.1638 0.0007 0.40	0.1633
Sample 26			0.2114
	11.4	0.2115 0.0002 0.08	0.2116
Sample 27			0.4491
	24.3 O	0.4493 0.0003 0.06	0.4495
Sample 28			0.4498
	24.4 O	0.4500 0.0003 0.07	0.4502